KILL ANALYSIS TOOL FOR MISSILES EQUIPPED WITH PROXIMITY FUZES

A THESIS SUBMITTED TO
THE GRADUATE SCHOOL OF NATURAL AND APPLIED SCIENCES
OF
MIDDLE EAST TECHNICAL UNIVERSITY

BY

ECE ÖZTÜRK

IN PARTIAL FULFILLMENT OF THE REQUIREMENTS
FOR
THE DEGREE OF MASTER OF SCIENCE
IN
AEROSPACE ENGINEERING

MARCH 2021

Approval of the thesis:

KILL ANALYSIS TOOL FOR MISSILES EQUIPPED WITH PROXIMITY FUZES

submitted by **ECE ÖZTÜRK** in partial fulfillment of the requirements for the degree of **Master of Science** i**n Aerospace Engineering, Middle East Technical University** by,

Prof. Dr. Halil Kalıpçılar

Dean, Graduate School of **Natural and Applied Sciences**

Prof. Dr. İsmail Hakkı Tuncer

Head of the Department, **Aerospace Engineering**

Assist. Prof. Dr. Ali Türker Kutay

Supervisor, **Aerospace Engineering Dept., METU**

Examining Committee Members:

Prof. Dr. Ozan Tekinalp

Aerospace Engineering Dept., METU

Assist. Prof. Dr. Ali Türker Kutay

Aerospace Engineering Dept., METU

Assoc. Prof. Dr. Utku Kanoğlu

Engineering Sciences Dept., METU

Assoc. Prof. Dr. İlkay Yavrucuk

Aerospace Engineering Dept., METU

Assist. Prof. Dr. Kutluk Bilge Arıkan

Mechanical Engineering Dept., TEDU

Date: 18.03.2021

I hereby declare that all information in this document has been obtained and presented in accordance with academic rules and ethical conduct. I also declare that, as required by these rules and conduct, I have fully cited and referenced all material and results that are not original to this work.

Name, Last name: Ece Öztürk

Signature:

ABSTRACT

KILL ANALYSIS TOOL FOR MISSILES EQUIPPED WITH PROXIMITY FUZES

Öztürk, Ece
Master of Science, Aerospace Engineering
Supervisor: Assist. Prof. Dr. Ali Türker Kutay

March 2021, 78 pages

In this thesis study, a developed kill analysis tool for the missiles having proximity fuzes is presented. Some of today's missiles have proximity fuze, and this type of missiles' warhead can be detonated not when the missile hits the target but at a certain distance.

The warhead consists of fragments, and the fragments scattered by the explosion's effect are intended to penetrate the target. A tool is needed for doing kill analysis in order to find the blasting time that the maximum number of fragments hit the target.

It is aimed to detonate the warhead at the right time during the missile-target engagement by doing kill analyses for different engagement conditions with the help of the developed tool. Then, the kill analysis results are embedded into the missile computer before the missile is launched.

Keywords: Kill Analysis, Probability of Kill, Proximity Fuze, Missile Vulnerability

ÖZ

YAKLAŞMA TAPALI FÜZELER İÇİN ÖLDÜRME ANALİZİ ARACI

Öztürk, Ece
Yüksek Lisans, Havacılık ve Uzay Mühendisliği
Tez Yöneticisi: Dr. Öğr. Üyesi Ali Türker Kutay

Mart 2021, 78 sayfa

Bu tez çalışmasında, yaklaşma tapaya sahip füzeler için geliştirilen öldürme analizi aracı sunulmuştur. Günümüzdeki füzelerin bir kısmı yaklaşma tapalı olup bu tip füzelerde; füze hedefe direkt çarptığında değil belli bir mesafe kala harp başlığı patlatılabilmektedir.

Harp başlığı parçacıklardan oluşmaktadır ve patlamanın etkisiyle saçılan parçacıkların hedefe nüfuz etmesi amaçlanmaktadır. En çok sayıda parçacığın hedefe isabet ettiği patlatma zamanını bulabilmek için öldürme analizinin yapılabileceği bir araca ihtiyaç duyulmaktadır.

Geliştirilen araç sayesinde farklı angajman koşulları için öldürme analizleri yapılarak, füze-hedef angajmanı sırasında doğru zamanda harp başlığının patlatılmasını hedeflenmektedir. Füze fırlatılmadan önce öldürme analizi sonuçları füze bilgisayarının içine gömülmektedir.

Anahtar Kelimeler: Öldürme Analizi, Öldürme Olasılığı, Yaklaşma Tapa, Füze Vurulabilirliği

To my beautiful family,

ACKNOWLEDGMENTS

First of all, I would like to express my gratitude to my supervisor Assist. Prof. Dr. Ali Türker Kutay for giving me an opportunity to work with him and for his guidance and comments throughout my study.

I would like to thank my colleagues at ROKETSAN Missile Industries Inc., who answered my questions and supported me throughout this study.

I want to thank my dear grandmother Şerife Öztürk and my dear grandfather Selahattin Öztürk who raised me with love. I wish you were among us.

Finally, my deepest gratitude to my family, my mother Ayşe Öztürk, my father Mehmet Öztürk, and my sister İpek Öztürk for being my family, making me feel like they are always with me, providing me their endless love, supporting and encourage me in all my life and also to my beloved husband Murat Uludağ for his understanding and patience, without his encouragement, I would not have been able to finish this work. I feel so lucky to be a part of them.

TABLE OF CONTENTS

LIST OF TABLES

TABLES

LIST OF FIGURES

FIGURES

LIST OF ABBREVIATIONS

ABBREVIATIONS	
AOA	Angle of Attack
DOF	Degree of Freedom
DCM	Direction Cosine Matrix
vs	Versus

LIST OF SYMBOLS

SYMBOLS

β	sideslip angle
α	angle of attack
ϕ	Euler roll angle
θ	Euler pitch angle
ψ	Euler yaw angle
$\hat{C}^{(i,b)}$	transformation matrix from body-fixed reference frame to inertial frame
l_w	warhead length
r	warhead radius
ϕ_f	fragment roll angle
V_M	missile speed
V_T	target speed
V_F	fragment speed
$P_{frag_x}^{(b)}$, $P_{frag_y}^{(b)}$, $P_{frag_z}^{(b)}$	fragment position on x,y, and z axes in body-fixed reference frame
$missvel_x, missvel_y, missvel_z$	missile velocity on x,y, and z axes in inertial reference frame
$targvel_x, targvel_y, targvel_z$	target velocity on x,y, and z axes in inertial reference frame

CHAPTER 1

INTRODUCTION

1.1 Objective of the Study

The warhead is detonable at any time from the moment the missile detects the target for missiles having a proximity fuze. For this reason, it is of great importance to detonate the warhead at a time that will cause more damage to the target and increase lethality after the missile detects the target.

This thesis aims to develop a tool that calculates the number of striking fragments to detonate the warhead when the maximum fragment hits the target to increase lethality after the missile has detected the target for surface-to-air missiles with a proximity fuze.

The analysis will be made by detonating the warhead at each time step after the missile detects the target, and the number of fragments hitting the target is calculated at corresponding times thanks to this tool. As a result of the analysis, when the highest number of fragments hits the target, the warhead will be detonated at this time, providing the possibility of achieving high lethality.

Kill analyses are made and tabulated for many different engagement conditions before the missile is launched. For the engagement condition encountered during the flight, the information on how many seconds the missile will detonate the warhead after detecting the target can be read from the table.

1.2 Literature Review

The utilization of missiles has been expanded for military activities since World War 2. Besides, missiles are anticipated to have a much more significant portion of military tasks in the future.

A missile-target engagement is recognizedly depicted in two phases. The first phase is named the missile flyout, and the second phase is called the endgame. The part of the engagement from missile launch to the terminal flight phase where the missile is in the target neighborhood is known as the missile flyout. The missile's target detection and ensuing warhead detonation are incorporated in the endgame phase. Also, under the missile-target engagement conditions, an assessment of the effectiveness of the damage instruments related to a warhead on the target at warhead detonation time is in part of the endgame phase [1].

The warhead detonation moment should be chosen in the best way for the missile to cause more damage to the target during the war. This detonation is provided by the fuze that the one of the missile part. In other words, fuze can be defined as a part of an artillery projectile that detonates the explosive charge and ideally would detonate the shell in the most optimum position to strike maximum damage [2].

Many types of fuze can be used in the missile industry. Proximity fuzes are considered the most common fuze utilized in artillery ammunition. This is a direct result of their favorable position of delivering the most extreme harm to the objects they manage [3]. Proximity fuze is utilized to improve the warhead blast's performance and increment the sufficient distance of fragmentation warhead [3].

The missile will almost certainly be passed close to the target without physically hitting it toward the end of the missile-target engagement. For these missiles, the warhead is equipped with a proximity fuze to harm the target. The target is detected, information about the target such as its position, velocity, and orientation are gained, and the warhead is exploded at a reasonable point to maximize the

obliterating probability of the target by crippling indispensable parts on the target by proximity fuze [4].

Finding the correct time to detonate the warhead is relied upon many parameters to increase the damage on the target. Missile and target velocities and attitudes, heading angle, miss distance and direction, target's vulnerable parts position, fragment density, and velocity are called some of them [4].

Kill probability calculation for the typical target is significant in finishing the design of the missile. Previously, the missile kill probability was calculated by the target practice to result in completing the design. Although this technique is basic and the outcome could be picked up from the first hand, some constraints can be seen. The first one of the constraints is called cost. An increase in the consumption of missiles and targets can be seen because practices are done. There is not much target practice of the missile. The second one is described as an extensive attack area. The truth of missile kill probability can not be reflected by limited target practice. Furthermore, this method is easily influenced by the dependability of the missile and artificial complication, etc. This method can be useful for group checks of finishing the design for the missile. The target practice result is not suitable for estimating missile kill probability in the attacking territory. In fact, missile kill probability is related to launch condition, battlefield environment, target maneuverability, and target electronic jamming. It is hard to ascertain missile kill probability while finishing the design [5].

Proper operation of the fuze causation an anti-air missile warhead to work viably is essential to the on the crest of a wave engagement of a target. Fuze performance is likewise described by the exact position at which the fuze triggers the warhead; this is not the same as the seeker case and is crucial for determining the missile fuze/warhead system's overall lethality [6].

As can be understood from the above studies, a tool is needed for determining the optimum time to burst the warhead. In this thesis, when the maximum fragments hit the target is assumed as the optimum time.

1.3 Scope

This thesis is organized into four chapters. The first chapter is the introduction. In this chapter, the objective of the study is explained, and the literature review is represented.

The methodology for the kill analysis tool is described in Chapter 2, which contains the target model, warhead model, velocity and position of the fragment, a plane equation passing through three points, where the vector intersects plane and intersection point is inside or outside of the triangle.

In Chapter 3, developed tool results are presented and discussed for scenarios with different target types and different engagement conditions. Also, Monte Carlo analysis is conducted to examine the effect of uncertainties on the results. Besides, the tool developed in this thesis is compared with another tool that calculates the number of fragments hitting the target when the warhead is detonated.

Finally, in Chapter 4, the study's conclusion is stated, and possible future work is mentioned.

CHAPTER 2

METHODOLOGY

A method has been developed to calculate the fragments that hit the target by scattering from the warhead with the warhead explosion. In this method, the surface of the target is formed from triangular-shaped patches with known three points. Then the equation of the plane passing through these three points is found. The scattered fragments are calculated as vectors, and the point where the vector intersects the plane is calculated. Then, it was checked whether this point is in the triangle. If the point is in a triangle, the fragment is considered to have hit the target. If it is not inside, it is evaluated as not struck.

2.1 Target Model

A cruise missile and a fighter have been chosen as the target model. The surface of the target models is made up of triangular-shaped patches with known three points. The selected sample cruise missile model with 150, 250, 350, 500, 1000, 1500, 2000, 3500, 5000, and 10000 triangle numbers are created to decide how many triangles the targets' surface will have.

The top, side, and front views of the selected sample cruise missile model with 150 triangle numbers are shown in Figure 2.1, Figure 2.2, and Figure 2.3, respectively.

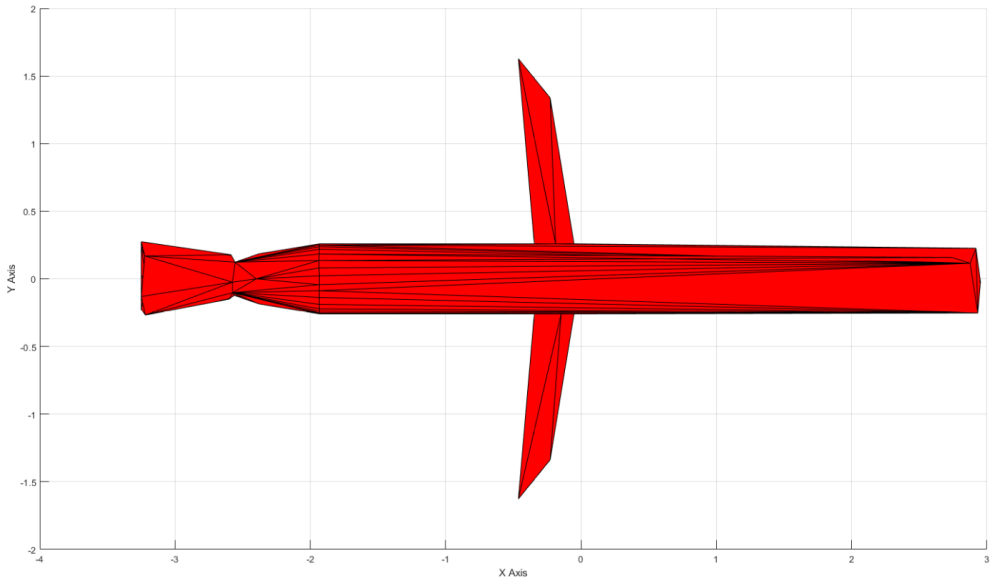

Figure 2.1: The Top View of the Cruise Missile with 150 Triangles in Total

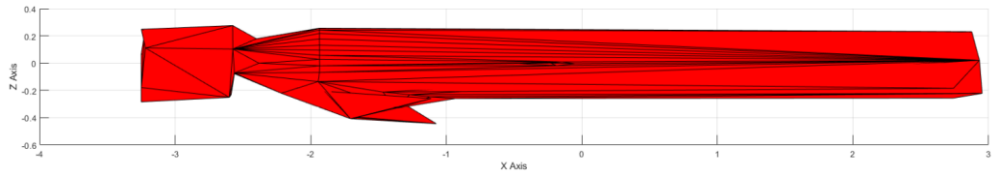

Figure 2.2: The Side View of the Cruise Missile with 150 Triangles in Total

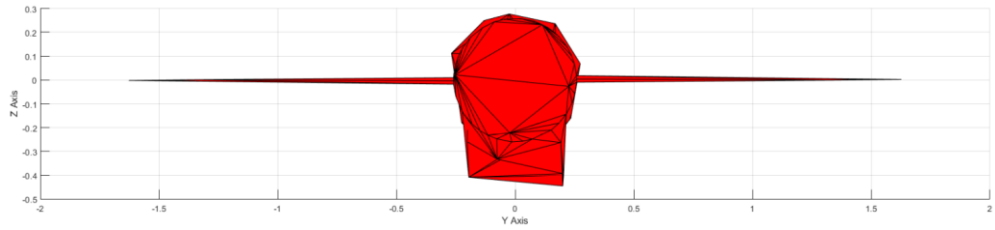

Figure 2.3: The Front View of the Cruise Missile with 150 Triangles in Total

The top, side, and front views of the selected sample cruise missile model with 250 triangle numbers are shown in Figure 2.4, Figure 2.5, and Figure 2.6, respectively.

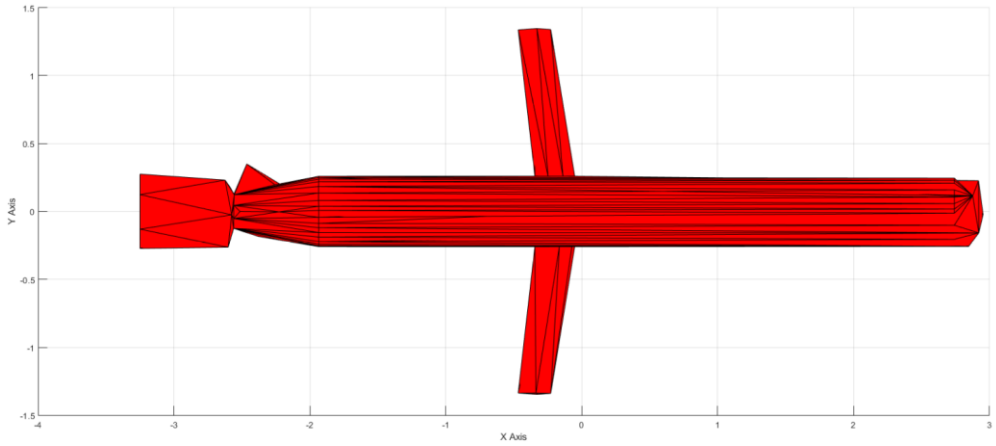

Figure 2.4: The Top View of the Cruise Missile with 250 Triangles in Total

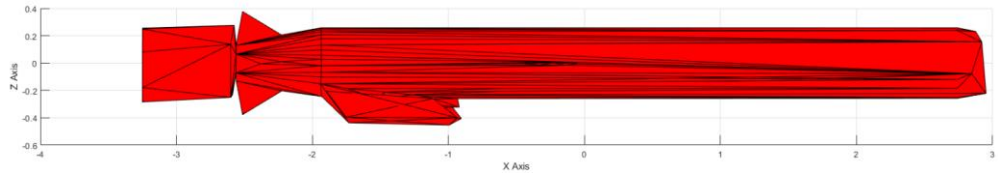

Figure 2.5: The Side View of the Cruise Missile with 250 Triangles in Total

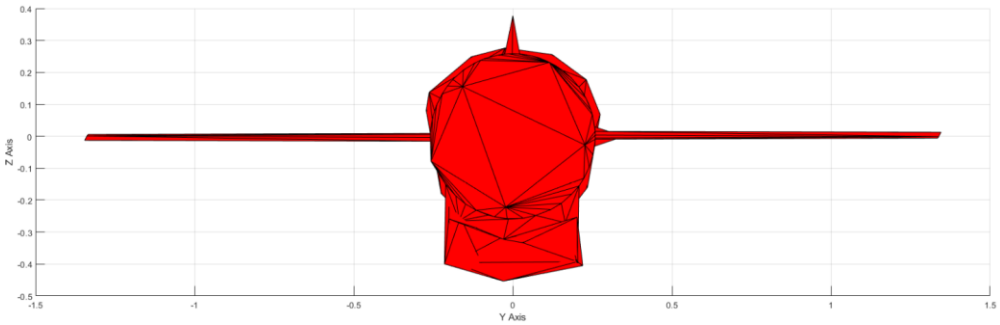

Figure 2.6: The Front View of the Cruise Missile with 250 Triangles in Total

The top, side, and front views of the selected sample cruise missile model with 350 triangle numbers are shown in Figure 2.7, Figure 2.8, and Figure 2.9, respectively.

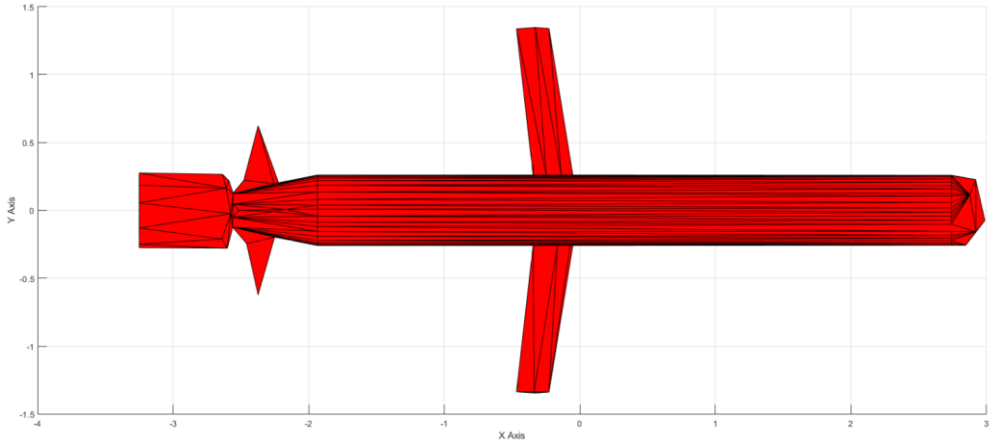

Figure 2.7: The Top View of the Cruise Missile with 350 Triangles in Total

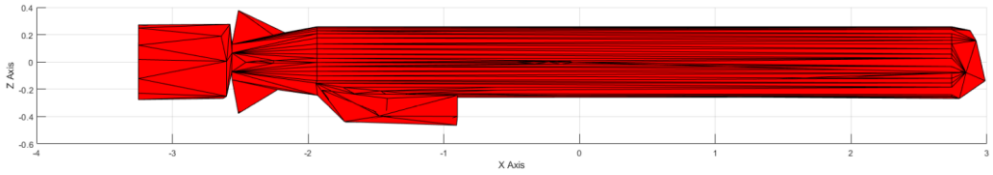

Figure 2.8: The Side View of the Cruise Missile with 350 Triangles in Total

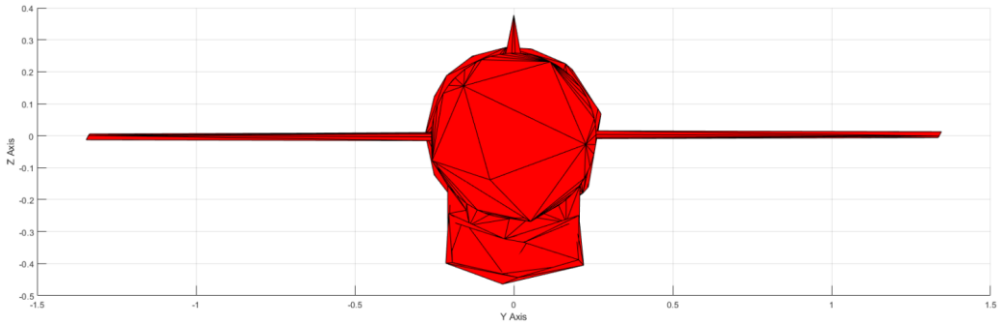

Figure 2.9: The Front View of the Cruise Missile with 350 Triangles in Total

The top, side, and front views of the selected sample cruise missile model with 500 triangle numbers are shown in Figure 2.10, Figure 2.11, and Figure 2.12, respectively.

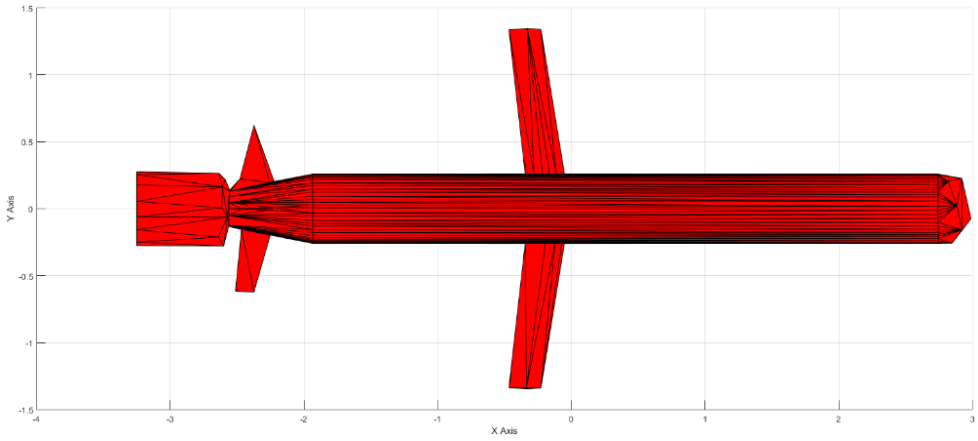

Figure 2.10: The Top View of the Cruise Missile with 500 Triangles in Total

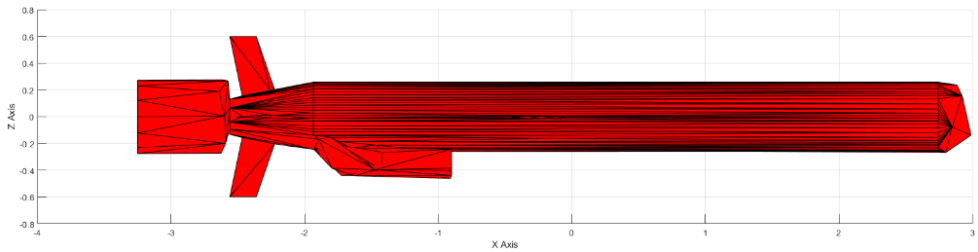

Figure 2.11: The Side View of the Cruise Missile with 500 Triangles in Total

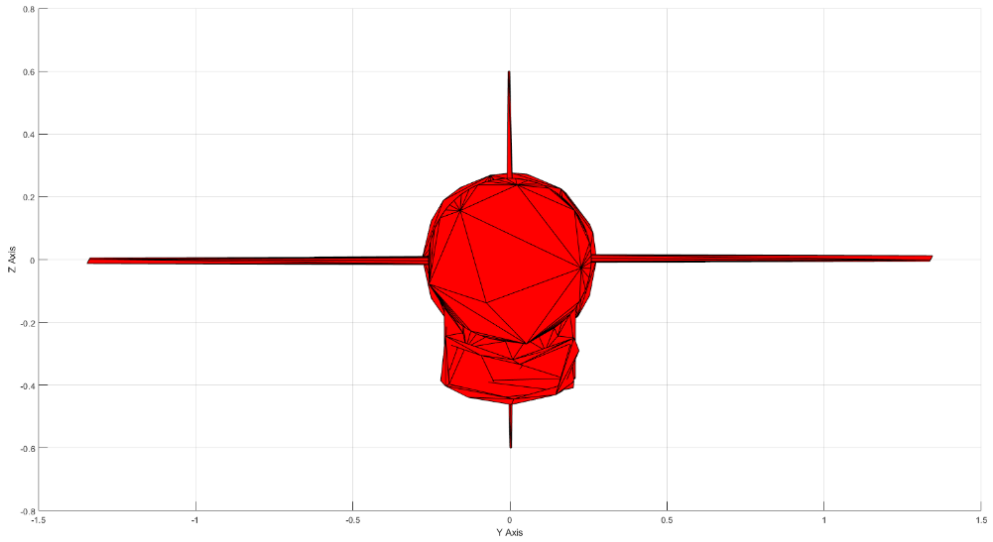

Figure 2.12: The Front View of the Cruise Missile with 500 Triangles in Total

The top, side, and front views of the selected sample cruise missile model with 1000 triangle numbers are shown in Figure 2.13, Figure 2.14, and Figure 2.15, respectively.

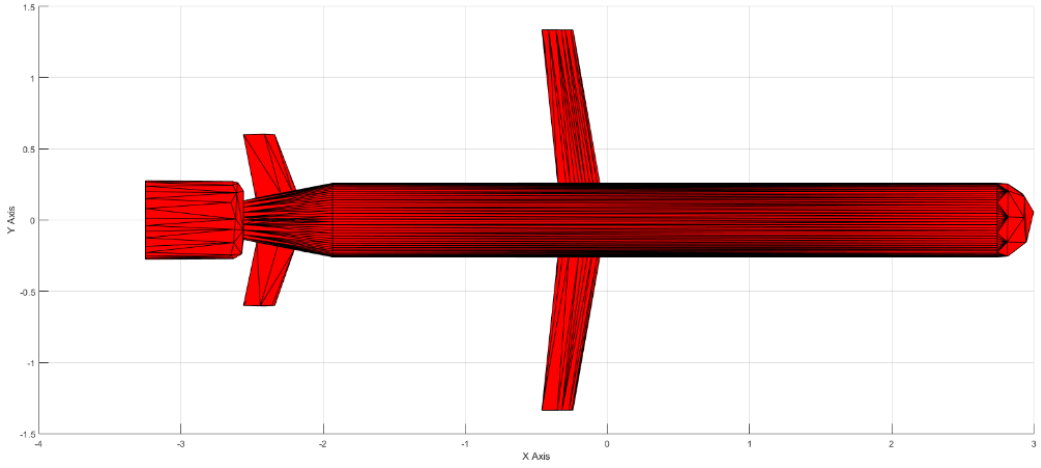

Figure 2.13: The Top View of the Cruise Missile with 1000 Triangles in Total

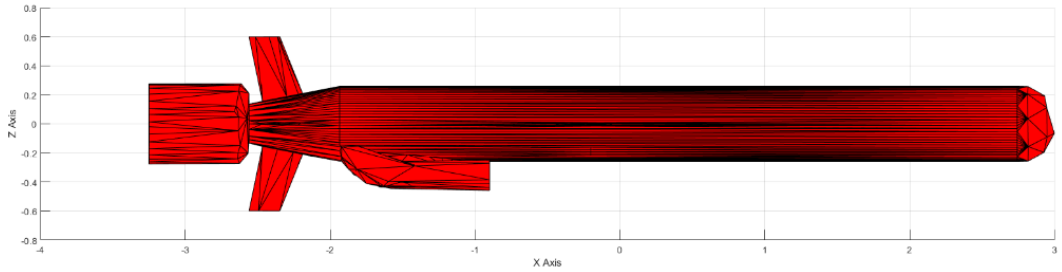

Figure 2.14: The Side View of the Cruise Missile with 1000 Triangles in Total

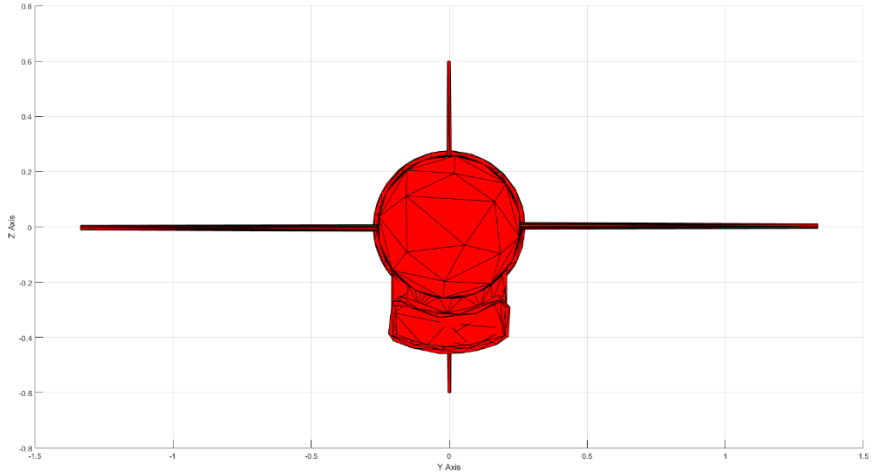

Figure 2.15: The Front View of the Cruise Missile with 1000 Triangles in Total

The top, side, and front views of the selected sample cruise missile model with 1500 triangle numbers are shown in Figure 2.16, Figure 2.17, and Figure 2.18, respectively.

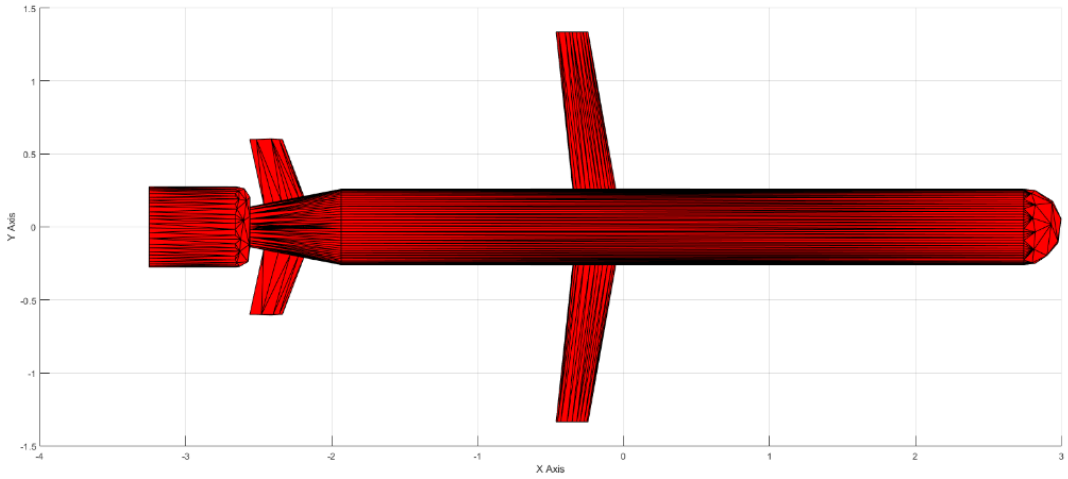

Figure 2.16: The Top View of the Cruise Missile with 1500 Triangles in Total

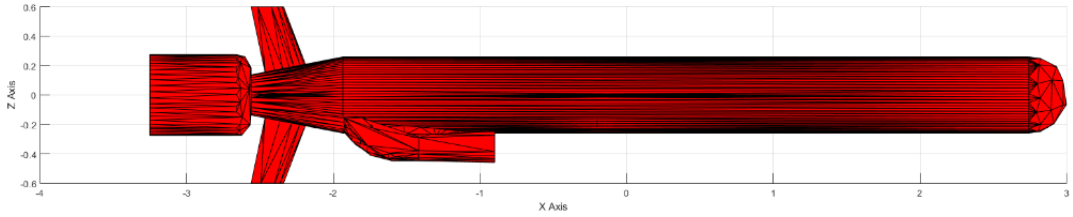

Figure 2.17: The Side View of the Cruise Missile with 1500 Triangles in Total

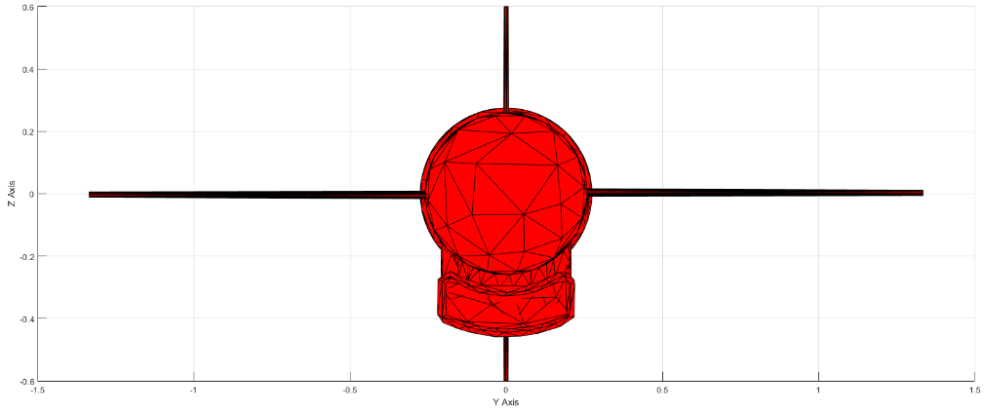

Figure 2.18: The Front View of the Cruise Missile with 1500 Triangles in Total

The top, side, and front views of the selected sample cruise missile model with 2000 triangle numbers are shown in Figure 2.19, Figure 2.20, and Figure 2.21, respectively.

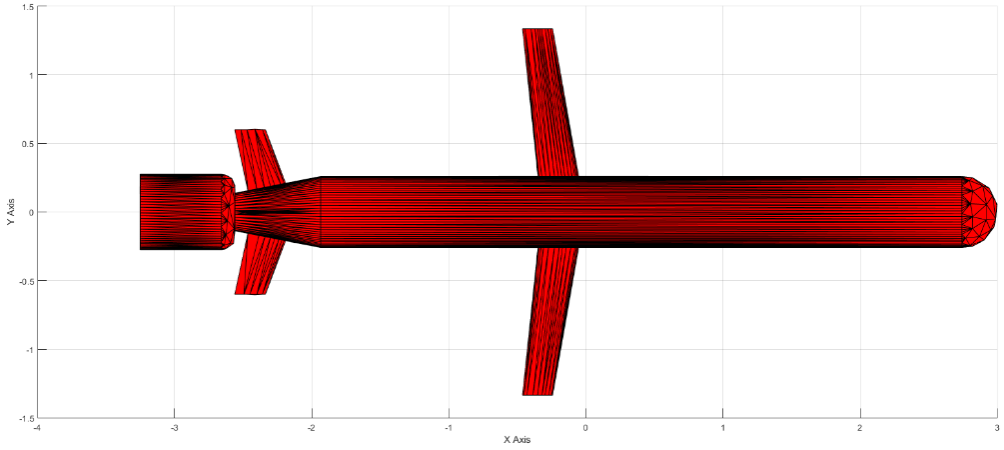

Figure 2.19: The Top View of the Cruise Missile with 2000 Triangles in Total

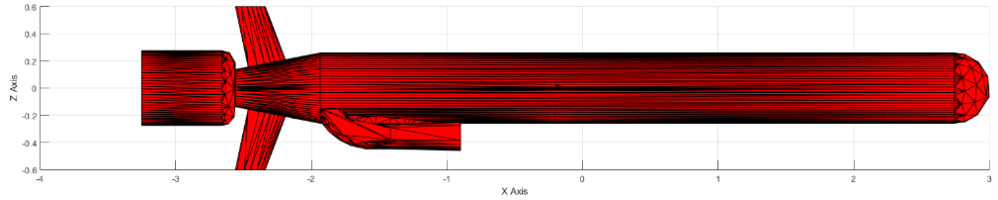

Figure 2.20: The Side View of the Cruise Missile with 2000 Triangles in Total

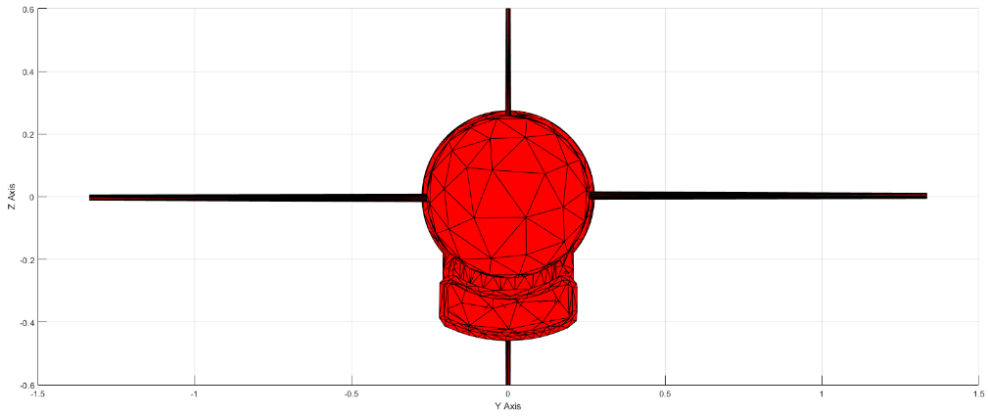

Figure 2.21: The Front View of the Cruise Missile with 2000 Triangles in Total

The top, side, and front views of the selected sample cruise missile model with 3500 triangle numbers are shown in Figure 2.22, Figure 2.23, and Figure 2.24, respectively.

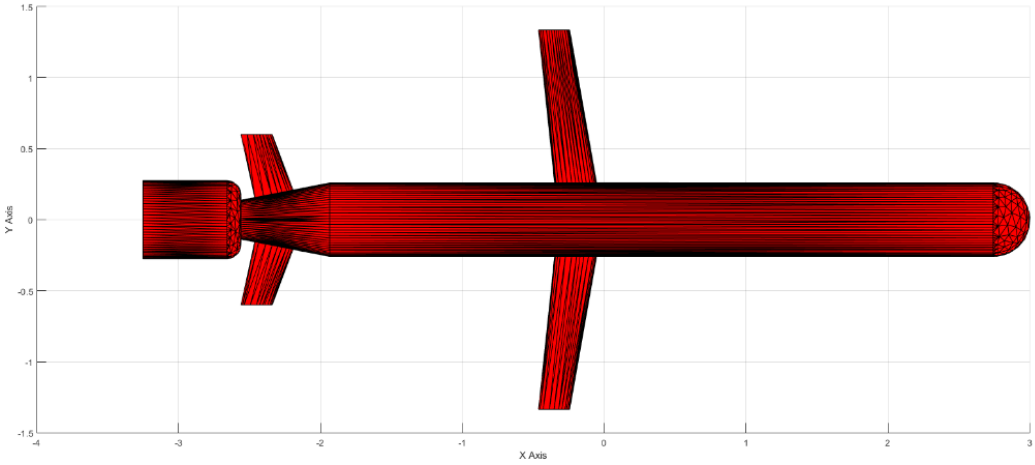

Figure 2.22: The Top View of the Cruise Missile with 3500 Triangles in Total

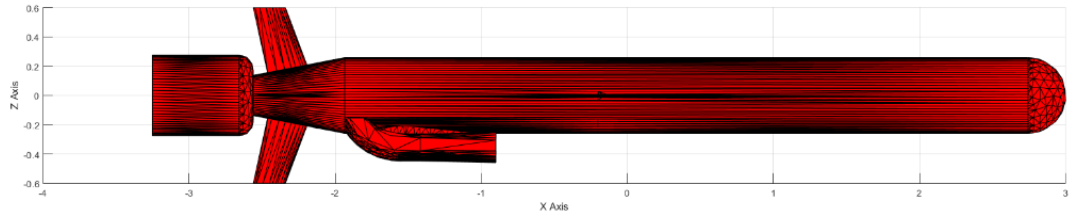

Figure 2.23: The Side View of the Cruise Missile with 3500 Triangles in Total

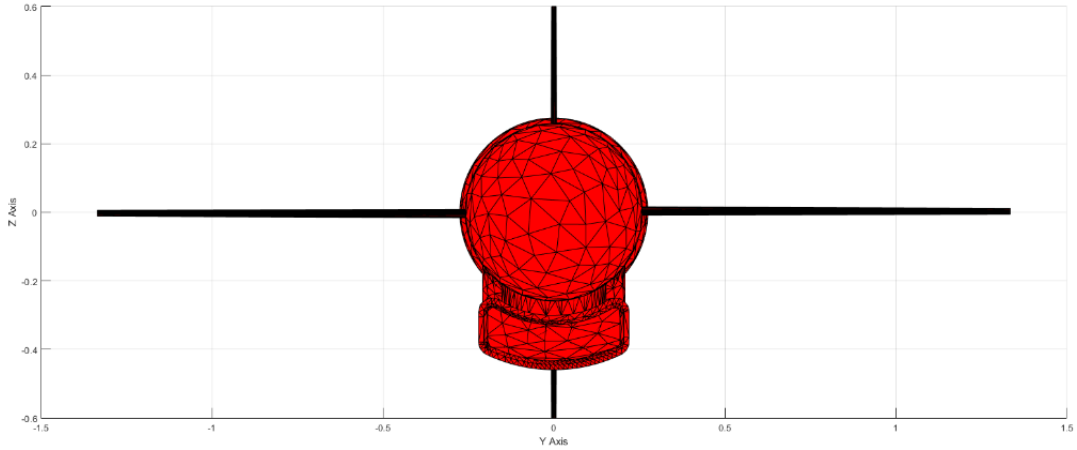

Figure 2.24: The Front View of the Cruise Missile with 3500 Triangles in Total

The top, side, and front views of the selected sample cruise missile model with 5000 triangle numbers are shown in Figure 2.25, Figure 2.26, and Figure 2.27, respectively.

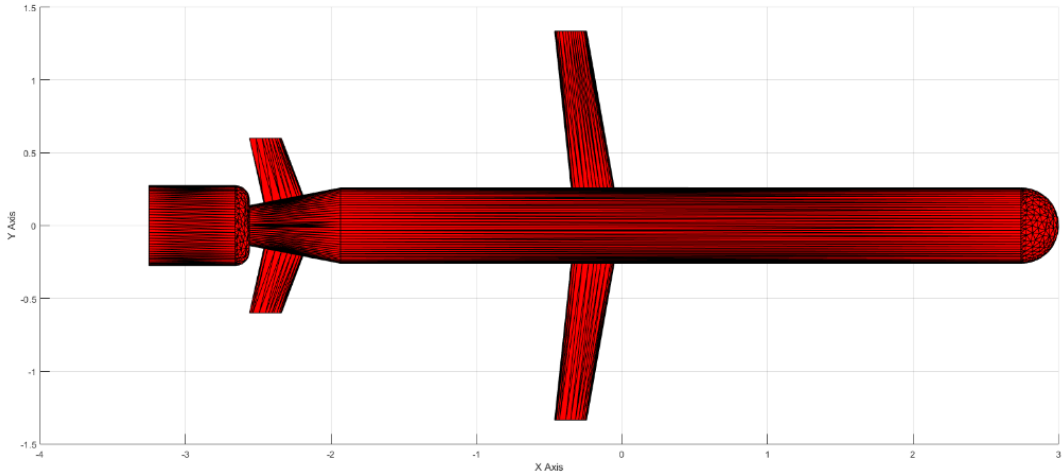

Figure 2.25: The Top View of the Cruise Missile with 5000 Triangles in Total

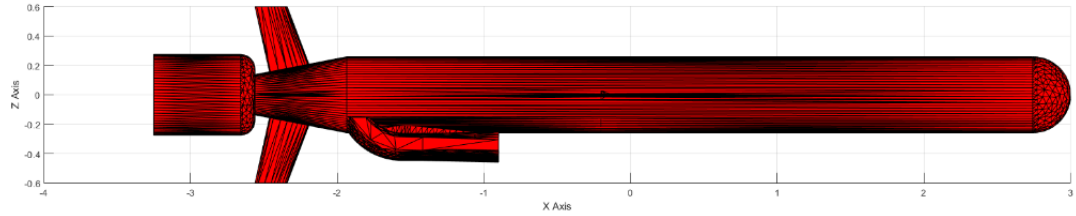

Figure 2.26: The Side View of the Cruise Missile with 5000 Triangles in Total

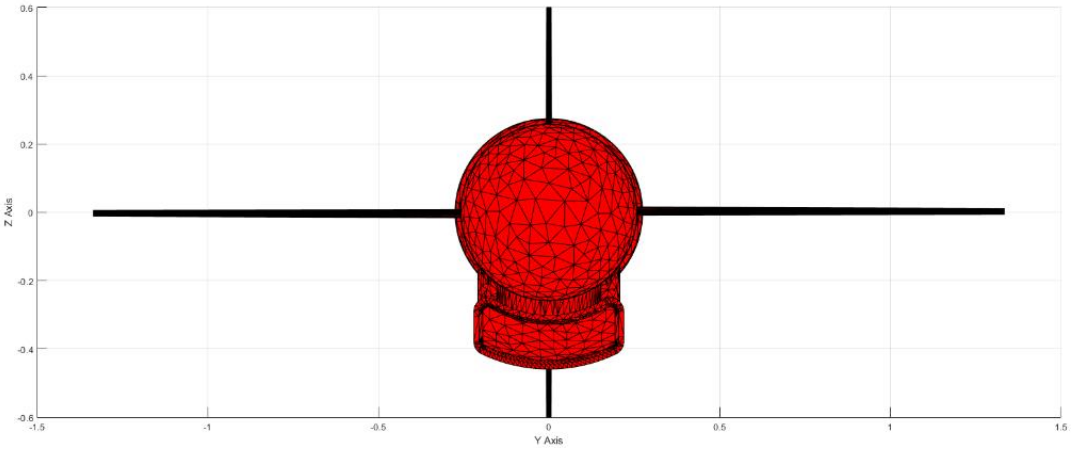

Figure 2.27: The Front View of the Cruise Missile with 5000 Triangles in Total

The top, side, and front views of the selected sample cruise missile model with 10000 triangle numbers are shown in Figure 2.28, Figure 2.29, and Figure 2.30, respectively.

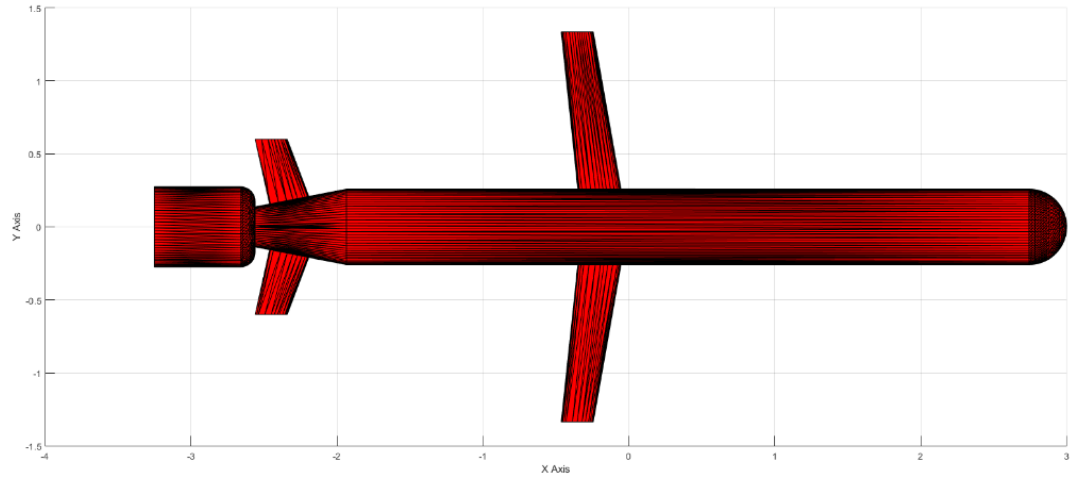

Figure 2.28: The Top View of the Cruise Missile with 10000 Triangles in Total

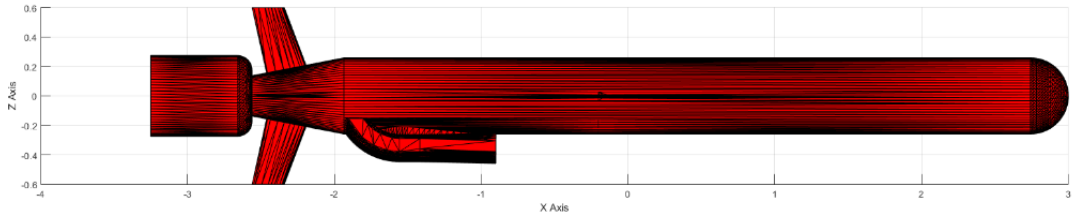

Figure 2.29: The Side View of the Cruise Missile with 10000 Triangles in Total

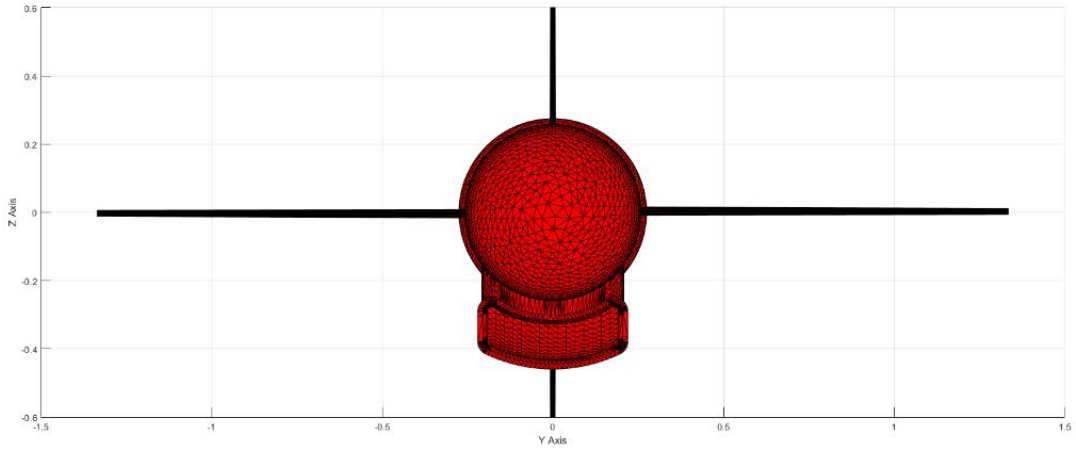

Figure 2.30: The Front View of the Cruise Missile with 10000 Triangles in Total

When the target surface triangle number is 150, 250, 350, 500, 1000, 1500, 2000, 3500, 5000, and 10000, kill analyses are made under exactly the same terminal conditions, and the results in Table 2.1 are obtained.

Table 2.1: Number of Fragments Hitting the Target and Simulation Time with respect to Total Triangle Numbers on the Target Surface

Total Triangle Number on the Target Surface:	**150**	**250**	**350**	**500**	**1000**	**1500**	**2000**	**3500**	**5000**	**10000**
No. of Fragments Hitting the Target @ Detonation Point 1	35	34	38	38	38	38	38	38	38	38
No. of Fragments Hitting the Target @ Detonation Point 2	37	37	40	41	41	41	41	41	41	41
No. of Fragments Hitting the Target @ Detonation Point 3	37	39	41	41	41	41	41	41	41	41
No. of Fragments Hitting the Target @ Detonation Point 4	37	40	41	41	41	41	41	41	41	41
No. of Fragments Hitting the Target @ Detonation Point 5	39	40	43	43	43	43	43	43	43	43
No. of Fragments Hitting the Target @ Detonation Point 6	42	42	46	46	46	46	46	46	46	46
No. of Fragments Hitting the Target @ Detonation Point 7	45	45	48	48	48	48	48	48	48	48
No. of Fragments Hitting the Target @ Detonation Point 8	57	55	56	56	54	54	54	54	54	54
No. of Fragments Hitting the Target @ Detonation Point 9	86	82	83	83	81	81	81	81	81	81
No. of Fragments Hitting the Target @ Detonation Point 10	85	84	84	84	84	84	84	84	84	84
No. of Fragments Hitting the Target @ Detonation Point 11	99	95	95	95	90	91	91	91	91	91
No. of Fragments Hitting the Target @ Detonation Point 12	97	101	101	101	101	101	101	101	101	101
No. of Fragments Hitting the Target @ Detonation Point 13	89	88	88	88	86	86	86	86	86	86
No. of Fragments Hitting the Target @ Detonation Point 14	56	57	57	57	57	57	58	58	58	58
No. of Fragments Hitting the Target @ Detonation Point 15	55	55	55	55	55	55	55	55	55	55
No. of Fragments Hitting the Target @ Detonation Point 16	55	55	55	55	55	55	55	55	55	55
No. of Fragments Hitting the Target @ Detonation Point 17	56	56	56	56	56	56	56	56	56	56
No. of Fragments Hitting the Target @ Detonation Point 18	57	57	57	57	57	57	57	57	57	57
No. of Fragments Hitting the Target @ Detonation Point 19	58	58	73	77	79	80	80	79	79	79
No. of Fragments Hitting the Target @ Detonation Point 20	52	59	58	58	72	73	73	71	71	72
No. of Fragments Hitting the Target @ Detonation Point 21	47	60	81	88	95	95	95	95	95	95
No. of Fragments Hitting the Target @ Detonation Point 22	47	66	77	80	80	80	81	81	81	81
No. of Fragments Hitting the Target @ Detonation Point 23	57	71	71	72	73	73	72	72	72	72
No. of Fragments Hitting the Target @ Detonation Point 24	45	52	55	56	57	57	57	57	57	57
No. of Fragments Hitting the Target @ Detonation Point 25	24	28	28	28	28	28	28	28	28	28
No. of Fragments Hitting the Target @ Detonation Point 26	0	0	0	0	0	0	0	0	0	0
Total Fragment Number Hitting the Target	1394	1456	1527	1544	1558	1561	1562	1559	1559	1560
Total Simulation Time (min)	3,02	5,17	6,85	11,16	22,35	33,41	51,30	134,55	212,65	449,40

It is seen from the figures that the more the number of triangles on the target surface, the more the model looks like the real one. On the other hand, when the results are examined in Table 2.1, it is seen that increasing the number of triangles does not dramatically affect the number of fragments hitting the target much. This is because analyses are done on the entire surface of the target.

Increasing the number of triangles also increases the simulation time as it is checked whether each fragment hits each triangle at each detonation point during the kill analyses. On the other hand, as the number of triangles on the target model is reduced, the model's details seem to disappear. For example, the engine's fins are started to deteriorate in the target model consisting of 500 triangles, and the fins on the engine are disappeared in the model composed of 150 triangles. Therefore, analyses are made by choosing a reasonable triangle number. 1000 is selected as the number of triangles where the analysis is performed.

The number of acceptable triangles on the target surface may differ in different target models. Since no significant deterioration is observed in the fighter model created with 1000 triangles, 1000 triangles are selected for this target type also.

The top, side, and front views of the chosen sample fighter model with 1000 triangle numbers are shown in Figure 2.31, Figure 2.32, and Figure 2.33, respectively.

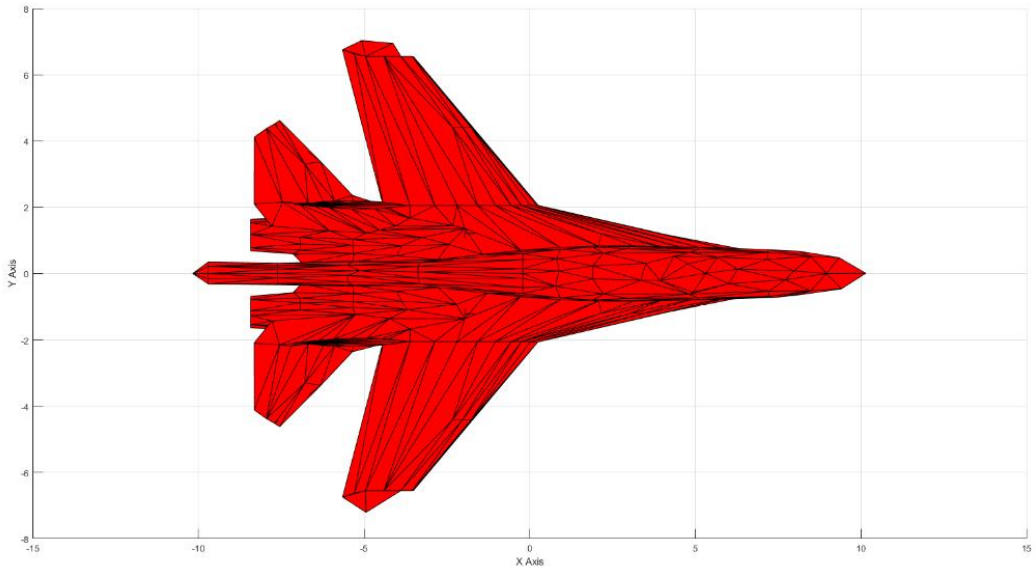

Figure 2.31: The Top View of the Fighter with 1000 Triangles in Total

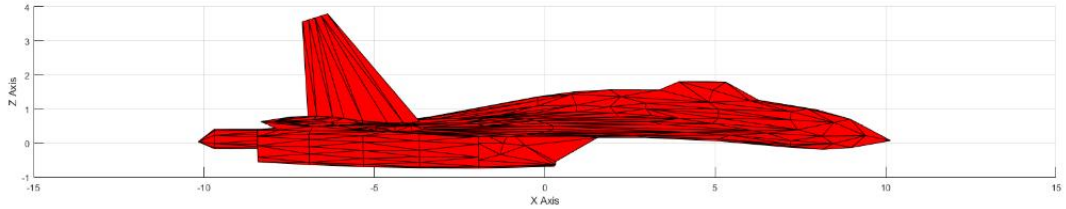

Figure 2.32: The Side View of the Fighter with 1000 Triangles in Total

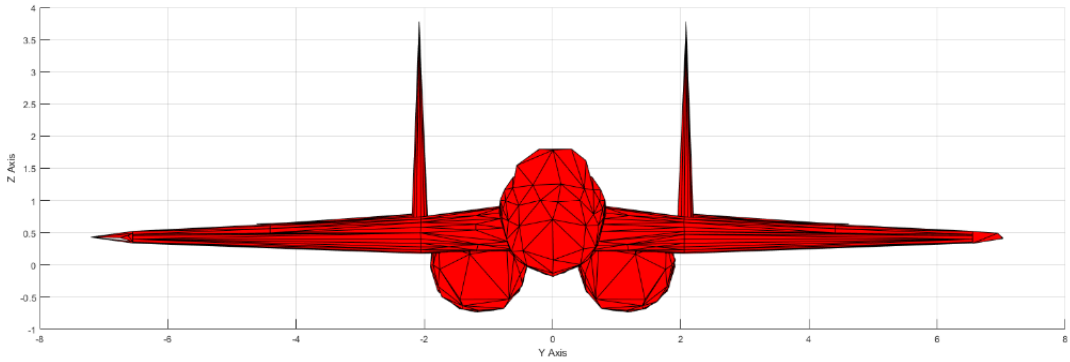

Figure 2.33: The Front View of the Fighter with 1000 Triangles in Total

2.2 Warhead Model

It is necessary to define some parameters such as number of segments, number of fragments, roll resolution, fragment number in one ring, number of the ring, fragment speeds, segment limits, warhead length, and warhead diameter to create the warhead model. These parameters and the values used in this thesis are defined as follows.

- Number of Segments

Each segment is defined with a fixed number of fragments, a fixed fragment speed, and a fixed elevation angular interval for the fragments.

The number of segments used in this thesis is:

$$segment_{number} = 4 \tag{2.1}$$

- Fragment Number

This parameter is defined as the number of fragments in each segment.

The number of fragments used in this thesis for the first segment is 360 fragments, for the second segment is 360 fragments, for the third segment is 180 fragments, and for the last and also the fourth segment is 240 fragments. The number of fragments belonging to each segment is shown as follows, respectively.

$$frag_{segment} = \begin{bmatrix} 360 & 360 & 180 & 240 \end{bmatrix} \tag{2.2}$$

The total number of fragments used for the warhead model is:

$$total_{fragment} = 1140 \tag{2.3}$$

- Roll Resolution

This parameter is defined as the roll angular resolution of all warhead fragments around the warhead. All fragments of the warhead are assumed to be uniformly distributed around the warhead frame roll axis.

Roll angle is taken in this thesis as:

$$roll_{angle} = 6^{\circ} \tag{2.4}$$

- Fragment Number in One Ring

Fragment number in one ring is defined by Roll Resolution. How many fragments will be in a ring can be learned from this parameter.

Because roll angle is taken as 6°, fragment number in one ring is equal to:

$$fragment_{ring} = 60 \tag{2.5}$$

- Ring Number

Each segment is made up of rings, and each ring is made up of fragments. Ring number can be calculated because the fragment number and roll resolution is known for each segment. Firstly, thanks to roll resolution, the fragment number in one ring can be calculated. Then, the fragment number in one segment is divided to fragment number in a one-ring, ring number can be found.

There is the number of rings according to segments, respectively:

$$ring_{segment} = \begin{bmatrix} 6 & 6 & 3 & 4 \end{bmatrix} \tag{2.6}$$

- Fragment Speeds

Fragment speed values can be defined for each segment. All fragments in a single segment will have the same speed.

The speed of fragments used in this thesis for the first segment is 900 m/s, for the second segment is 1100 m/s, for the third segment is 1100 m/s, and for the last and fourth segment is 1300 m/s. The speed of fragments belonging to each segment is shown as follows, respectively.

$$speed_{segment} = \begin{bmatrix} 900 & 1100 & 1100 & 1300 \end{bmatrix} m/s \tag{2.7}$$

- Segment Limits

This vector is defined as the elevation angular limits of each warhead segment. Fragments in a segment are ejected with a uniform angular distribution in between the segment limits. This vector has to include an exact 90° breakpoint. n+1 breakpoints define n segments. Because segment number is four, there are five-segment limits taken as:

$$segment_{\lim} = \left[80^{\circ} \quad 85^{\circ} \quad 90^{\circ} \quad 88^{\circ} \quad 86^{\circ} \right] \tag{2.8}$$

- Warhead Length

Warhead length is selected as:

$$l_w = 0.102m \tag{2.9}$$

- Warhead Diameter

A cylindrical warhead model with a diameter is chosen as:

$$d_w = 0.18m \tag{2.10}$$

The features of the warhead model used in this thesis are summarized in Table 2.2:

Table 2.2: Warhead Model Parameters

Total Fragment Number	1140 pieces
Roll Angle of Fragments in the Ring	6°
Fragment Number in One-Ring	60 pieces
Total Ring Number	19 pieces
Warhead Length	102 mm
Warhead Diameter	180 mm

The front, top, and side views of the selected warhead model are shown in Figure 2.34, Figure 2.35, and Figure 2.36, respectively.

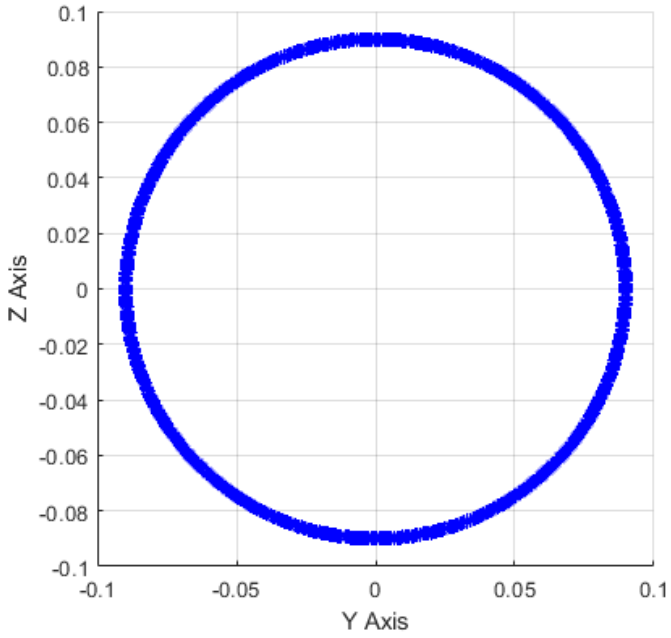

Figure 2.34: Warhead Model on YZ Axis

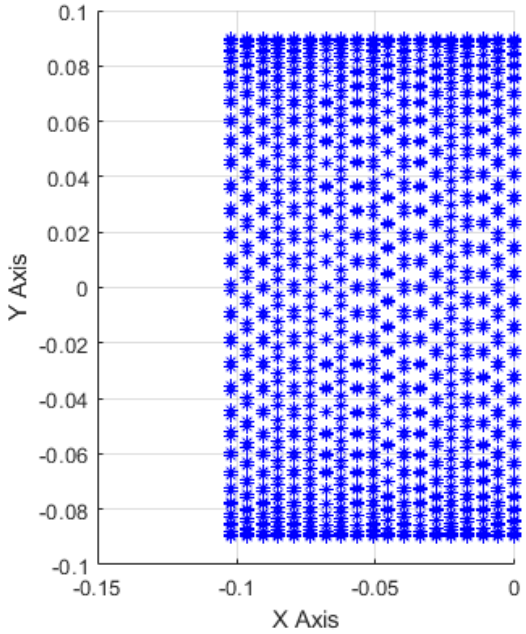

Figure 2.35: Warhead Model on XY Axis

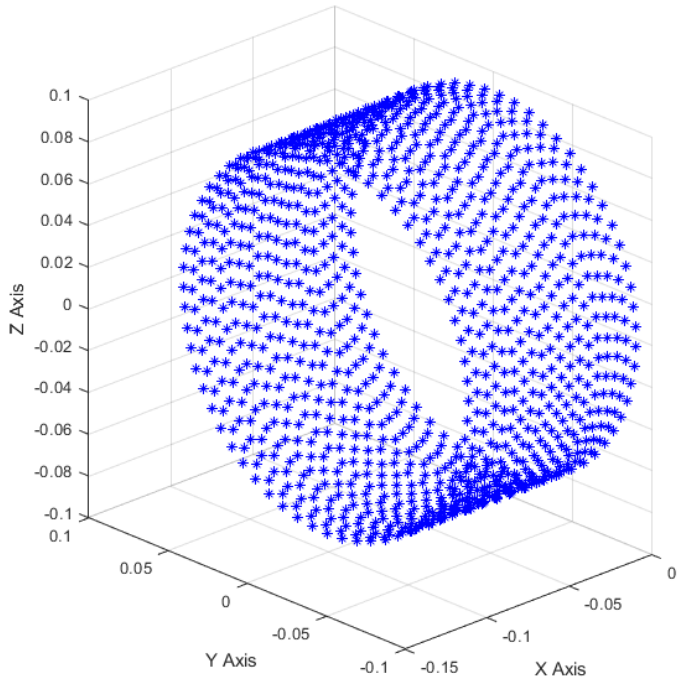

Figure 2.36: Warhead Model on XYZ Axis

Some parameters are shown on the warhead model as in Figure 2.37 and Figure 2.38 to make the parameters more understandable. The seg is used as an abbreviation of the segment in Figure 2.37.

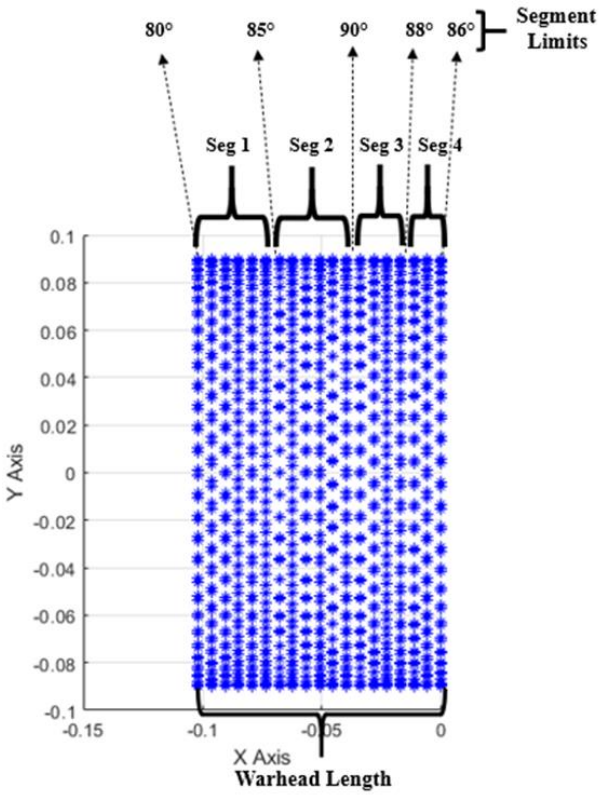

Figure 2.37: Representation of Some Warhead Parameters on the XY Axis of the Warhead Model

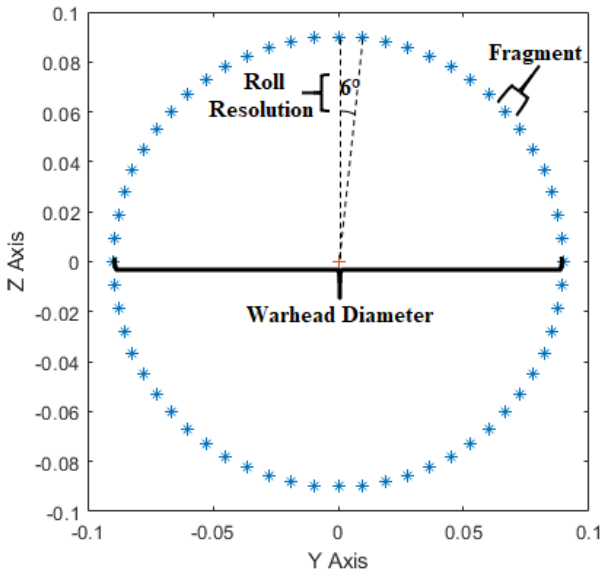

Figure 2.38: Representation of Some Warhead Parameters on One Ring

2.3 Fragment Velocity and Position

The kill analysis tool is needed to velocity and position of the fragments with respect to the target in the inertial reference frame at the detonation points.

2.3.1 Fragment Velocity

The speed, AOA, sideslip angle, and Euler angles of the missile and target are known from the 6 DOF simulation output. All transactions performed in the kill analysis tool are made relative to the target in the inertial reference frame. For this, the velocity of the missile, target, and warhead fragments must be expressed in the inertial frame.

Transformation is made from one coordinate reference frame to another using DCM. The transformation matrix in the Eqn.(2.11) is obtained using Euler angles by the 3-2-1 Euler ordered transformation to transform the inertial reference frame to a body-fixed reference frame. The names of the Euler angles are yaw, pitch, roll and their symbols ψ, θ, ϕ, respectively.

$$C_{ZYX}(\psi,\theta,\phi) = C^{(b,i)} = \hat{R}_3(\phi)\hat{R}_2(\theta)\hat{R}_1(\psi) \tag{2.11}$$

Where,

$$\hat{R}_1(\psi) = \begin{bmatrix} \cos\psi & \sin\psi & 0 \\ -\sin\psi & \cos\psi & 0 \\ 0 & 0 & 1 \end{bmatrix} \tag{2.12}$$

$$\hat{R}_2(\theta) = \begin{bmatrix} \cos\theta & 0 & -\sin\theta \\ 0 & 1 & 0 \\ \sin\theta & 0 & \cos\theta \end{bmatrix} \tag{2.13}$$

$$\hat{R}_3(\phi) = \begin{bmatrix} 1 & 0 & 0 \\ 0 & \cos\phi & \sin\phi \\ 0 & -\sin\phi & \cos\phi \end{bmatrix} \tag{2.14}$$

Eqn.(2.12), Eqn.(2.13) and Eqn.(2.14) is putted into the Eqn.(2.11):

$$C^{(b,i)} = \begin{bmatrix} 1 & 0 & 0 \\ 0 & \cos\phi & \sin\phi \\ 0 & -\sin\phi & \cos\phi \end{bmatrix} \begin{bmatrix} \cos\theta & 0 & -\sin\theta \\ 0 & 1 & 0 \\ \sin\theta & 0 & \cos\theta \end{bmatrix} \begin{bmatrix} \cos\psi & \sin\psi & 0 \\ -\sin\psi & \cos\psi & 0 \\ 0 & 0 & 1 \end{bmatrix} \tag{2.15}$$

Then,

$$C^{(b,i)} = \begin{bmatrix} \cos\theta\cos\psi & \cos\theta\sin\psi & -\sin\theta \\ \sin\phi\sin\theta\cos\psi - \cos\phi\sin\psi & \sin\phi\sin\theta\sin\psi + \cos\phi\cos\psi & \sin\phi\cos\theta \\ \cos\phi\sin\theta\cos\psi + \sin\phi\sin\psi & \cos\phi\sin\theta\sin\psi - \sin\phi\cos\psi & \cos\phi\cos\theta \end{bmatrix} \tag{2.16}$$

$\hat{C}^{(b,i)}$is called the direction cosine matrix representing the transformation from the inertial frame to a body frame. $\hat{C}^{(b,i)}$is an orthogonal transformation matrix; thus Eqn. (2.17) can be written as:

$$C^{(i,b)} = C^{(b,i)^{-1}} = C^{(b,i)^T} \tag{2.17}$$

$$C^{(i,b)} = \begin{bmatrix} \cos\theta\cos\psi & \sin\phi\sin\theta\cos\psi - \cos\phi\sin\psi & \cos\phi\sin\theta\cos\psi + \sin\phi\sin\psi \\ \cos\theta\sin\psi & \sin\phi\sin\theta\sin\psi + \cos\phi\cos\psi & \cos\phi\sin\theta\sin\psi - \sin\phi\cos\psi \\ -\sin\theta & \sin\phi\cos\theta & \cos\phi\cos\theta \end{bmatrix}$$

(2.18)

The missile speed is represented by V_M and the Eqn. (2.19) is used to write the velocity of the missile in the missile body-fixed frame. Sideslip angle is denoted as β, and angle of attack is denoted as α.

$$\overline{v}_M^{(b)} = C_{ZYX}(-\beta, \alpha, 0) \begin{bmatrix} V_M \\ 0 \\ 0 \end{bmatrix} \tag{2.19}$$

Where,

$$C_{ZYX}(-\beta,\alpha,0)=\begin{bmatrix}\cos(\alpha) & 0 & -\sin(\alpha)\\ 0 & 1 & 0\\ \sin(\alpha) & 0 & \cos(\alpha)\end{bmatrix}\begin{bmatrix}\cos(-\beta) & \sin(-\beta) & 0\\ -\sin(-\beta) & \cos(-\beta) & 0\\ 0 & 0 & 1\end{bmatrix} \quad (2.20)$$

Missile speed is expressed in the wind-fixed frame. Transformation is done from wind fixed frame of reference to body-fixed reference frame using DCM in the Eqn. (2.20).

Transformation is done from body-fixed reference frame to inertial frame in Eqn. (2.21) to express the missile velocity in the inertial frame of reference:

$$\bar{v}_M^{(i)} = C^{(i,b)}\bar{v}_M^{(b)} \quad (2.21)$$

The same calculations are done for the target. Target speed is represented by V_T.

Then,

$$\bar{v}_T^{(i)} = C^{(i,b)}C_{ZYX}(-\beta,\alpha,0)\begin{bmatrix}V_T\\ 0\\ 0\end{bmatrix} \quad (2.22)$$

It is assumed that the target has no angle of attack and no sideslip angle. In this case, $\hat{C}_{ZYX}(-\beta,\alpha,0)$ is turned to identity matrix and the target velocity can be calculated in the inertial reference frame as in the Eqn.(2.23).

$$\bar{v}_T^{(i)} = C^{(i,b)}\begin{bmatrix}V_T\\ 0\\ 0\end{bmatrix} \quad (2.23)$$

As a result of these calculations, missile and target velocities in the inertial reference frame are found.

In addition, the relative velocity of fragments to the target must be found in the inertial reference frame.

The initial speed that the fragments will gain from the explosion is defined and denoted as V_F. Fragment speeds vary from segment to segment, and the speed of fragments in the same segment are considered the same. These fragment speeds should also be expressed in the inertial frame as $\vec{V}_F^{(i)}$. DCM matrix is needed for finding $\vec{V}_F^{(i)}$. Two different DCM should be obtained according to the segment angular limit. Segment limits are taken as [80° 85° 90° 88° 86°] is mentioned in Eqn. (2.8).

Fragments in front of the ninety-degree segment limit are scattered forward. Thus, the DCM matrix for these fragments can be written as in Eqn. (2.24). Fragment roll angle is denoted as ϕ_f, and the pitch angle of the fragment in the ring is denoted as θ_r. Fragments in the same ring have the same pitch angle.

$$C^{(f,b)} = C_{ZXY}(0, \phi_f, \theta_r) \tag{2.24}$$

Fragments behind the ninety-degree segment limit are scattered to the back. Thus, the DCM matrix for these fragments can be written as in Eqn.(2.25).

$$C^{(f,b)} = C_{ZXY}(\pi, -\phi_f, \theta_r) \tag{2.25}$$

For the last segment, pitch angles of the rings are calculated in Eqn.(2.27) and shown as seg_{vector}. By using Eqn. (2.26), The pitch angle difference from one ring to another ring Δseg can be found. The number of the ring in the segment is shown as $ring_{seg}$ .The segment limits of the segment are shown as seg_1 and seg_2.

$$\Delta seg = \frac{seg_2 - seg_1}{ring_{segment} - 1} \tag{2.26}$$

Then,

$$seg_{vector} = seg_1 : \Delta seg : seg_2 \tag{2.27}$$

For the other segments, pitch angles of the rings are calculated in Eqn. (2.29).

$$\Delta seg = \frac{seg_2 - seg_1}{ring_{segment}} \tag{2.28}$$

$$seg_{vector} = seg_1 : \Delta seg : seg_2 - \Delta seg \tag{2.29}$$

The seg_{vector} is written in two different ways so that there is no ring with the same pitch angle.

$\hat{C}^{(f,b)}$is an orthogonal transformation matrix, so Eqn.(2.30) can be written:

$$C^{(f,b)^T} = C^{(b,f)} \tag{2.30}$$

Then, fragment velocity is expressed as in body-fixed frame by using Eqn. (2.31).

$$\overline{v}_F^{(b)} = C^{(b,f)} \begin{bmatrix} V_F \\ 0 \\ 0 \end{bmatrix} \tag{2.31}$$

As a result of these, the relative velocity of the fragments to the target in the inertial frame can be calculated using Eqn.(2.32).

$$\overline{v}_{TF}^{(i)} = \overline{v}_M^{(i)} + C^{(i,b)} \overline{v}_F^{(b)} - \overline{v}_T^{(i)} \tag{2.32}$$

Since the velocity, Euler angles, AOA, and the sideslip angle do not change much in milliseconds, they are assumed to be the same at each detonation point. Therefore, it is sufficient to calculate the velocity of the fragments for the first detonation point.

2.3.2 Fragment Position

The kill analysis tool is needed to fragment positions with respect to the target in the inertial reference frame at the detonation points.

The missile position relative to the target at the time of detection is known in the inertial frame from the simulation output. This distance is the distance between the

CG of the missile and the target. The position of the warhead relative to the target and the position of fragments relative to the warhead must be found to find the initial position of the fragments relative to the target. In Eqn.(2.33), TF abbreviation is used to mean relative position of the fragment to target , TW abbreviation is used to mean relative position of the warhead to target, and WF abbreviation is used to mean relative position of the fragment to the warhead.

$$\vec{P}_{TF}^{(i)} = \vec{P}_{TW}^{(i)} + \vec{P}_{WF}^{(i)} \tag{2.33}$$

Where,

$$\vec{P}_{TW}^{(i)} = \vec{P}_{TM}^{(i)} + \vec{P}_{MW}^{(i)} \tag{2.34}$$

Since $\vec{P}_{TM}^{(i)}$ is known, $\vec{P}_{TW}^{(i)}$ can be found if $\vec{P}_{MW}^{(i)}$ is calculated.

The distance of the warhead's front tip with respect to the CG of the missile is defined in the missile body-fixed frame and is shown as $P_{MW}^{(b)}$. The CG of the missile is adopted where the target detection sensor is.

To be found $\vec{P}_{MW}^{(i)}$;

$$\overline{P}_{MW}^{(i)} = C^{(i,b)}\overline{P}_{MW}^{(b)} \tag{2.35}$$

In this way, the position of the warhead relative to the missile is found in the inertial reference frame.

Since the positions of the missile relative to the target ($\vec{P}_{TM}^{(i)}$) and the warhead relative to the missile ($\vec{P}_{MW}^{(i)}$) are known in the inertial frame, the position of the warhead relative to the target ($\vec{P}_{TW}^{(i)}$) can be found in the inertial frame by using Eqn. (2.34).

$\vec{P}_{TW}^{(i)}$ is the position of the fragments at the first detonation point.

Since the position of the fragments at the first detonation point is known, it can be calculated at other detonation points by using Eqn. (2.36).

$$\vec{P}_{TW_n}^{(i)} = \vec{P}_{TW}^{(i)} + \vec{V}_{TM}^{(i)} * (n-1) * d_t \tag{2.36}$$

The detonation point is expressed as n, the relative velocity vector of the missile to the target $\vec{V}_{TM}$ and the time elapsed between two detonation points is expressed as d_t in Eqn. (2.36).

The $\vec{V}_{TM}^{(i)}$ is found by using Eqn. (2.21) and Eqn. (2.23) as in Eqn. (2.37).

$$\vec{V}_{TM}^{(i)} = \vec{v}_M^{(i)} - \vec{v}_T^{(i)} \tag{2.37}$$

The distance between the two detonation points must be determined as one of the kill analysis tool inputs. This distance is denoted as $det_{interval}$.

Then, d_t is calculated as in Eqn. (2.38):

$$d_t = \frac{\det_{interval}}{\left|\vec{V}_{TM}^{(i)}\right|} \tag{2.38}$$

After the warhead position with respect to the target is found for each detonation point, the fragments' position to the warhead should be calculated. If $P_{WF}^{(i)}$ is found, $P_{TF}^{(i)}$ can be found.

Since the diameter of the warhead and roll angle of the fragments on the warhead are known, their positions on the y and z-axis can also be found using Eqn.(2.39) and Eqn.(2.40), respectively. The fragment roll angle is indicated as $\emptyset_f$, warhead radius is indicated as *r*, fragment's position on y-axis and on z-axis is expressed as $P_{frag_y}^{(b)}$ and $P_{frag_z}^{(b)}$, respectively, in Figure 2.39.

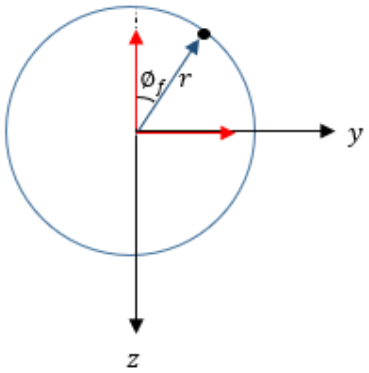

Figure 2.39: Fragment Position on the Ring

$$P_{frag_y}^{(b)} = r * \sin\phi_f \tag{2.39}$$

$$P_{frag_z}^{(b)} = -r * \cos\phi_f \tag{2.40}$$

The position of the ring where the fragment is located must be known to find the fragment's position on the x-axis. The fragments' position in the ring on the x-axis is the same as the position of the ring on the x-axis.

The position of a ring, in other words, the position of the fragment on the x-axis relative to the front of the warhead, can be written in Eqn. (2.41):

$$P_{frag_x}^{(b)} = -(ring_{number} - 1)\frac{l_W}{ring_{total} - 1} \tag{2.41}$$

In the Eqn. (2.41) the fragment x-axis position is denoted by $P_{frag_x}^{(b)}$, the ring number is denoted by $ring_{number}$, the warhead length is denoted by l_w and the total number of rings is denoted by $ring_{total}$.

Then, the position of fragments can be written as follows:

$$\vec{P}_{WF}^{(b)} = \begin{bmatrix} -(ring_{number} - 1)\dfrac{l_W}{ring_{total} - 1} \\ r * \sin\phi_f \\ -r * \cos\phi_f \end{bmatrix} \tag{2.42}$$

To be expressed in the inertial reference frame of the fragment position:

$$\vec{P}_{WF}^{(i)} = C^{(i,b)}\vec{P}_{WF}^{(b)} \tag{2.43}$$

As a result of these, $\vec{P}_{TF}^{(i)}$ can be calculated by using Eqn. (2.33).

2.4 Finding the Equation of a Plane Passing Through 3 Points

If three points on a plane are known, the equation of the plane can be found by using the following steps.

Let $P(x_1, y_1, z_1), Q(x_2, y_2, z_2)$ and $R(x_3, y_3, z_3)$ be the three points of a triangle on the target model's surface.

The equation of a plane in three-dimensional space is as follows:

$$a(x - x_0) + b(y - y_0) + c(z - z_0) = 0 \tag{2.44}$$

Where (x_0, y_0, z_0) is a point on the plane and $< a, b, c >$ is a vector that perpendicular to the plane.

$\overrightarrow{PQ}$ and $\overrightarrow{PR}$ should be defined as:

$$\overrightarrow{PQ} = \langle (x_2 - x_1), (y_2 - y_1), (z_2 - z_1) \rangle \tag{2.45}$$

$$\overrightarrow{PR} = \langle (x_3 - x_1), (y_3 - y_1), (z_3 - z_1) \rangle \tag{2.46}$$

To find $< a, b, c >$,

$$\overrightarrow{PQ} \times \overrightarrow{PR} = \begin{pmatrix} i & j & k \\ (x_2 - x_1) & (y_2 - y_1) & (z_2 - z_1) \\ (x_3 - x_1) & (y_3 - y_1) & (z_3 - z_1) \end{pmatrix} = \langle a, b, c \rangle \quad (2.47)$$

This process is done for all triangles on the target model. There are 1000 triangles on the selected target model's surface. One thousand plane equations are represented by these 1000 triangles. After finding the plane equations expressed by the triangles, it should be calculated that at which point the fragments scattered from the warhead intersect the planes.

2.5 Finding the Point Where the Vector Intersects the Plane

First of all, the fragment scattered from the warhead should be expressed as a vector. The fragment's first position and any second position along its path are needed to express a fragment as a vector because two points are required to define the vector.

The general formula of the vector equation of a line passing through two points as follows:

$$\bar{r}(h) = \bar{r_0} + h(\bar{v}) \quad (2.48)$$

Where,

$\bar{r_0} = \langle x_0, y_0, z_0 \rangle$ is an initial point of the vector (2.49)

h is the direction vector coefficient

$\bar{v} = \langle (x_1 - x_0), (y_1 - y_0), (z_1 - z_0) \rangle$ is a direction vector, where $< x_1, y_1, z_1 >$ is a second point of the vector (2.50)

Let put Eqn. (2.49) and Eqn. (2.50) into the Eqn. (2.48):

$$\bar{r}(h) = \langle x_0, y_0, z_0 \rangle + h\langle (x_1 - x_0), (y_1 - y_0), (z_1 - z_0) \rangle \quad (2.51)$$

Then,

$$x(h) = x_0 + h(x_1 - x_0) \quad (2.52)$$

$$y(h) = y_0 + h(y_1 - y_0) \quad (2.53)$$

$$z(h) = z_0 + h(z_1 - z_0) \quad (2.54)$$

When Eqn.(2.52), Eqn.(2.53) and Eqn.(2.54) are putted into the Eqn.(2.44), h is found.

$$a(x_0 + h(x_1 - x_0) - x_0) + b(y_0 + h(y_1 - y_0) - y_0) + c(z_0 + h(z_1 - z_0) - z_0) = 0 \quad (2.55)$$

If the finding h is written into the Eqn.(2.52), Eqn.(2.53) and Eqn.(2.54), the point where the vector intersects the plane can be calculated.

The following situations have been taken into consideration while finding the intersection point of the fragment vector and plane.

- Parallel Checking

The fragment vector should not be parallel to the plane because if the fragment vector and the plane are parallel, they will not intersect. For checking this, the dot product of the normal of the plane and the direction vector of the fragment vector is calculated. If the dot product value is 0, the angle between normal and direction vector is 90 degrees, and it means the vector is parallel to the plane. In other words, the value of the dot product should not be equal to 0 for the vector not to be parallel to the plane. Those with a dot product value of zero were eliminated, and the process continued.

Before finding out whether the point where the fragment intersects the plane is in the triangle, the following case is considered. This case is applied to us choosing valid intersection points.

❖ Behind Checking

The coefficient of the direction vector must be calculated to finding an acceptable intersection point.

When the direction vector's coefficient is negative, the triangle is behind the direction vector's origin, causing the intersection point to be opposite to the fragment vector's direction. These cases should be eliminated because there is no valid intersection.

2.6 Finding Out Whether the Point Where the Fragment Intersects the Plane is in the Triangle

Let Q be the point where the fragment vector intersects the plane formed by the 3 points of the triangle, and the normal of the plane is defined as $\vec{n}$.

Examples of point Q inside and outside of the triangle are shown in Figure 2.40 and Figure 2.41, respectively.

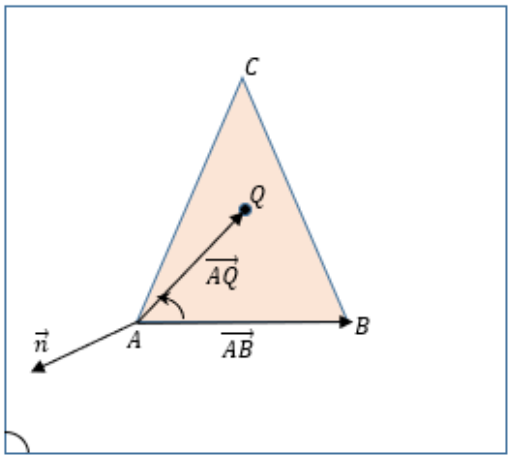

Figure 2.40: Point Q is Inside the Triangle

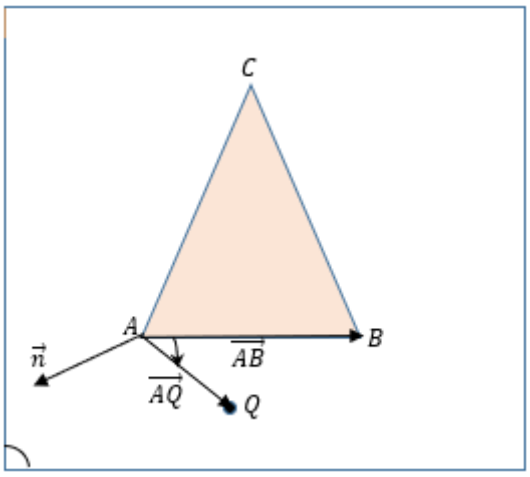

Figure 2.41: Point Q is Outside the Triangle

To say that the Q point is in a triangle, it must simultaneously fulfill the following three conditions, which are Eqn.(2.56), Eqn.(2.57) and Eqn.(2.58).

$$\left[(B-A)\times(Q-A)\right]\bullet\vec{n}\geq 0 \tag{2.56}$$

$$\left[(C-B)\times(Q-B)\right]\bullet\vec{n}\geq 0 \tag{2.57}$$

$$\left[(A-C)\times(Q-C)\right]\bullet\vec{n}\geq 0 \tag{2.58}$$

When these conditions are provided, the fragment will be deemed to have hit the target.

A fragment vector may have hit more than one triangle, so it is necessary to look at which triangle is hit first. For this, if the fragment hits more than one triangle, it is taken into account that the distance between the initial position of the fragment vector and the point where the fragment intersects triangles are examined, and the fragment first hits the triangle with the shortest distance to its initial position.

CHAPTER 3

RESULTS AND DISCUSSION

3.1 Problem Definition

In this thesis, the number of impacting fragments to the target at each detonation point is calculated for different scenarios using the developed tool. Firstly, kill analysis is done for a cruise missile in the first scenario and for a fighter in the second scenario to show that the tool is worked with different target types. Then, in addition to the original miss distance value in the first scenario, kill analyses are performed for the first scenario with 14 different miss distances to see different engagement conditions' effects on the results. After that, the Monte Carlo analyses are performed with 50 runs for observing the impact of the warhead model uncertainties on the results. Finally, kill analysis is done for the first scenario by using another tool in the industry, and the results are compared with the developed tool in this thesis.

The velocities, Euler angles, AOA, sideslip angle, and positions of the missile and the target at the miss distance are known as the 6 DOF simulation output. Miss distance is defined as the shortest distance between the missile and the target.

Since the velocity, Euler angles, AOA, and the sideslip angle do not change much in milliseconds, they are assumed to be the same at each detonation point. Positions have been changed at each detonation point.

In addition, the missile's target detection range and the information of the position of the missile to the target at the time of detection in the inertial reference frame are known. The missile's target detection range is the path taken by the missile on the relative velocity vector. The calculations are made relative to the target because it provides ease of operation as the target will be accepted as standing.

3.2 Results and Discussion

3.2.1 The First Scenario

The first scenario is chosen as a cruise missile arriving at an altitude of 30 meters and a speed of 250 m/s.

In the first scenario, the missile and target speed, Euler angles, AOA, and sideslip angle at the time of engagement are in Table 3.1.

Table 3.1: Missile and Target Kinematics for the 1^{st} Scenario

	Missile	**Target**
Speed	642.9 m/s	250 m/s
Roll Angle (ϕ)	-1.94 °	0
Pitch Angle (θ)	-36.48 °	0
Yaw Angle (ψ)	1.28 °	180 °
AOA (α)	-20.92 °	0
Sideslip Angle(β)	-0.14 °	0

In this scenario, the target is detected by the missile while the missile is ~ 3.1 m away from the target. Detection distance is denoted by det_{dist}.

Analyses are made along the path twice the distance the missile detected the target. The reason for this is to analyse along with the target.

Then, the total distance at which the analyses are carried out:

$$total_{dist} = \det_{dist} * 2 \tag{3.1}$$

$$total_{dist} = 3.1 * 2 = 6.2m \tag{3.2}$$

The kill analysis is carried out at every 0.25 m along the 6.2 m road, including when the missile detected the target. Thus, the total number of detonation points is calculated as follows:

$$No.of\ \det_{point} = \frac{total_{dist} - 0}{\det_{interval}} + 1 \tag{3.3}$$

$$No.of\ \det_{point} = \frac{6.2 - 0}{0.25} + 1 = \sim 26 \tag{3.4}$$

How many fragments hit the target for each detonation point can be seen from Table 3.2 as the kill analysis tool output.

Table 3.2: Detonation Point vs Number of Fragments Hitting the Target for the 1^{st} Scenario

Detonation Point	**1**	**2**	**3**	**4**	**5**	**6**	**7**	**8**	**9**	**10**	**11**	**12**	**13**
No. of Fragments Hitting the Target	38	41	41	41	43	46	48	54	81	84	90	101	86
Detonation Point	**14**	**15**	**16**	**17**	**18**	**19**	**20**	**21**	**22**	**23**	**24**	**25**	**26**
No. of Fragments Hitting the Target	57	55	55	56	57	79	72	95	80	73	57	28	0

Fragments hitting the target at each detonation point can be seen from Figure 3.1, Figure 3.2, and Figure 3.3. Each detonation point is shown in a different colour. The first detonation point starts from the missile's nose, and the other detonation points are shown on the relative velocity vector for 6.2 meters at 0.25 m intervals.

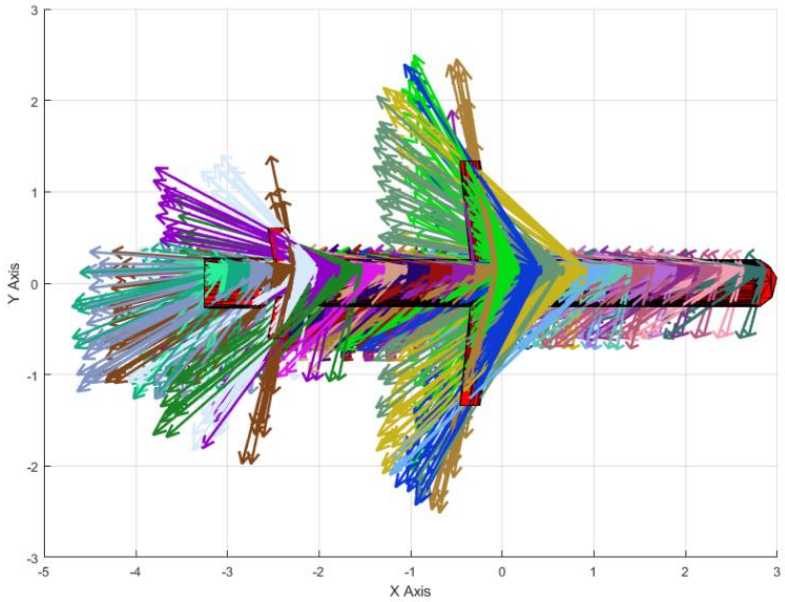

Figure 3.1: Scattering of Striking Fragments at All Detonation Points on XY Axis for the 1^{st} Scenario

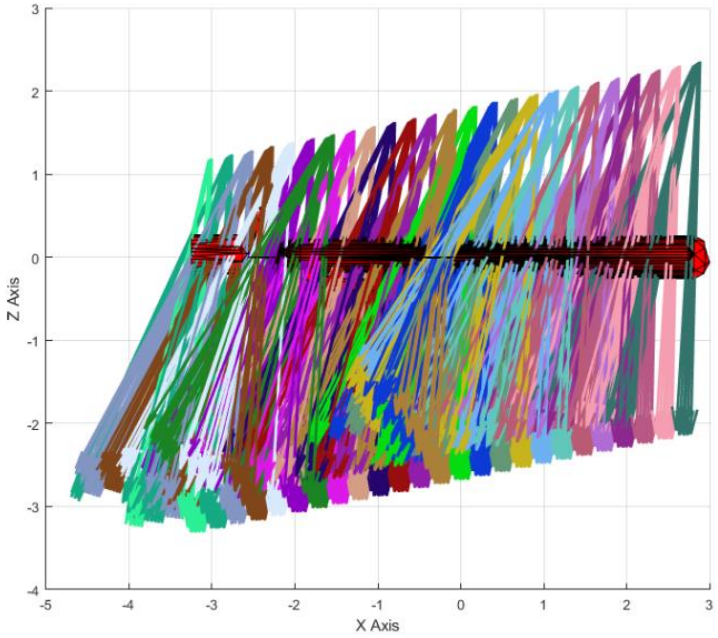

Figure 3.2: Scattering of Striking Fragments at All Detonation Points on XZ Axis for the 1^{st} Scenario

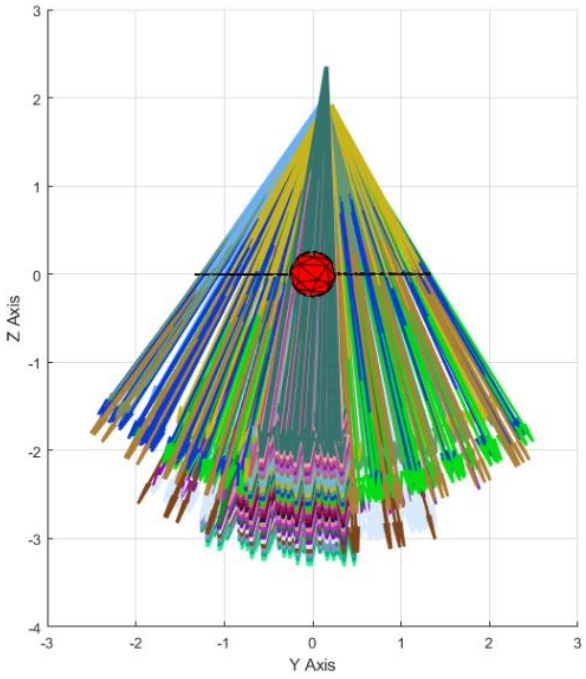

Figure 3.3: Scattering of Striking Fragments at All Detonation Points on YZ Axis for the 1^{st} Scenario

As can be seen from Table 3.2, the target is hit mostly by the fragment at the detonation point 12.

The scattering plot of the fragments hitting the target at the twelfth detonation point can be seen in Figure 3.4, Figure 3.5, and Figure 3.6.

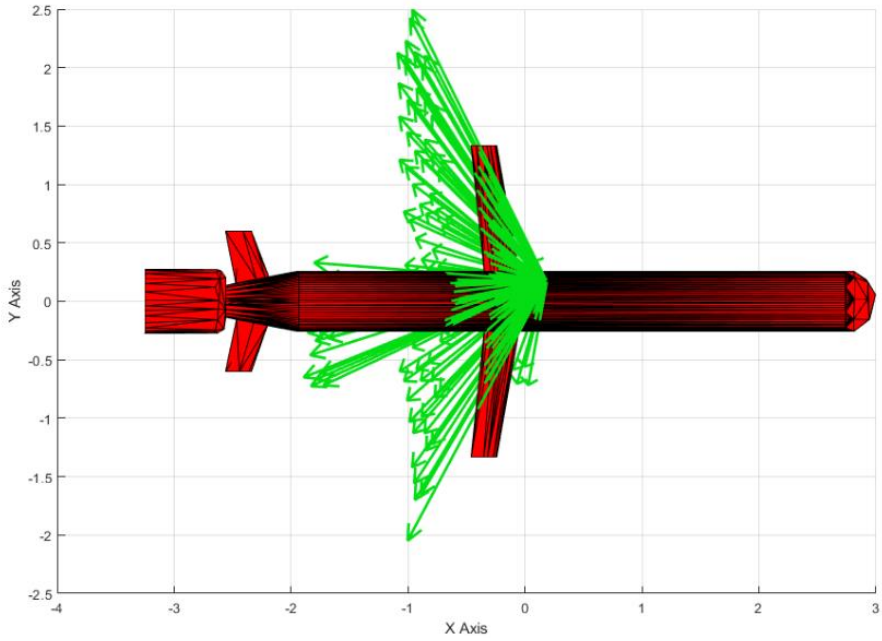

Figure 3.4: Scattering of Striking Fragments at Detonation Point 12 on XY Axis for the 1^{st} Scenario

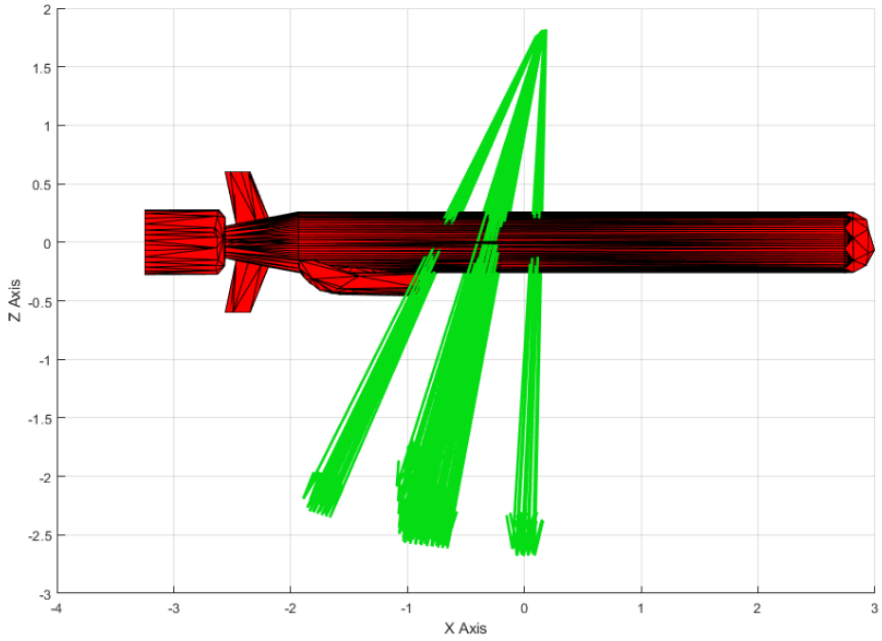

Figure 3.5: Scattering of Striking Fragments at Detonation Point 12 on XZ Axis for the 1^{st} Scenario

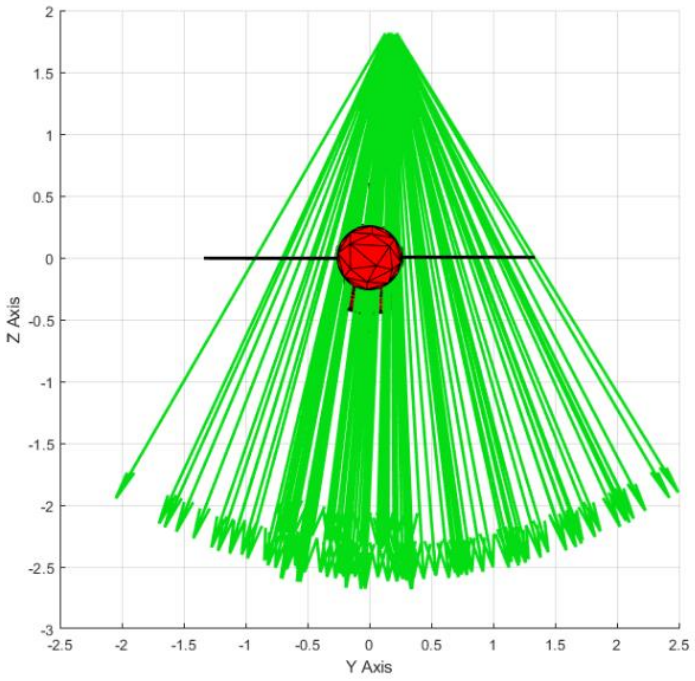

Figure 3.6: Scattering of Striking Fragments at Detonation Point 12 on YZ Axis for the 1^{st} Scenario

The scattering plot of all fragments, including fragments non-hitting the target at the twelfth detonation point can be seen from Figure 3.7, Figure 3.8 and Figure 3.9.

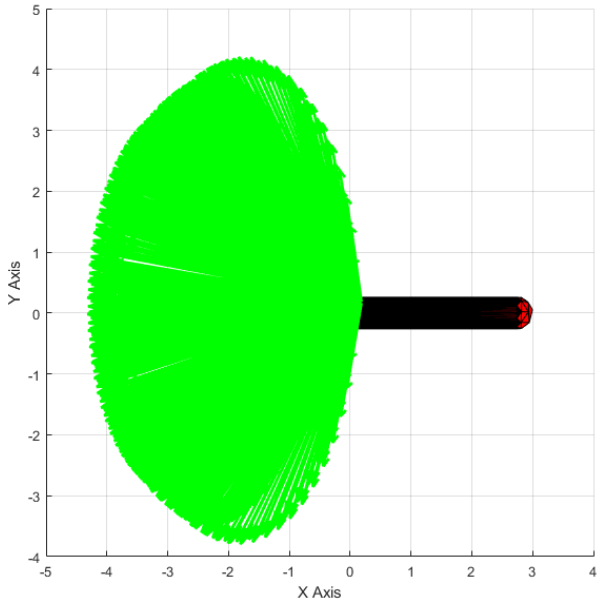

Figure 3.7: Scattering of All Fragments at Detonation Point 12 on XY Axis for the 1^{st} Scenario

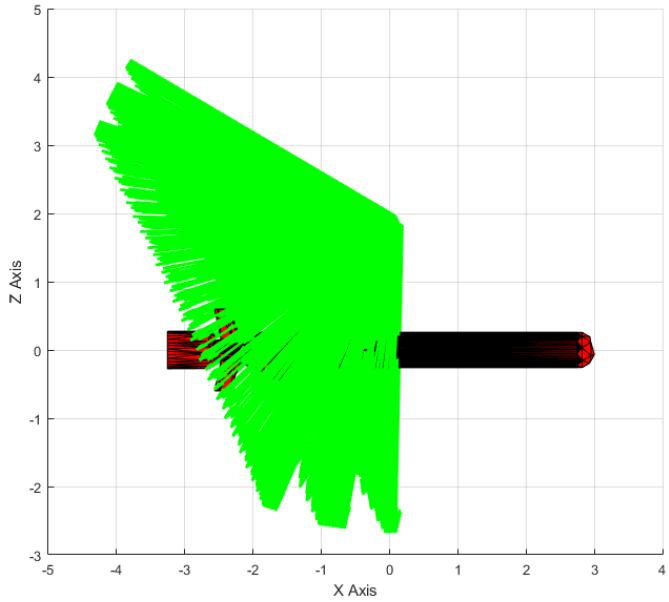

Figure 3.8: Scattering of All Fragments at Detonation Point 12 on XZ Axis for the 1^{st} Scenario

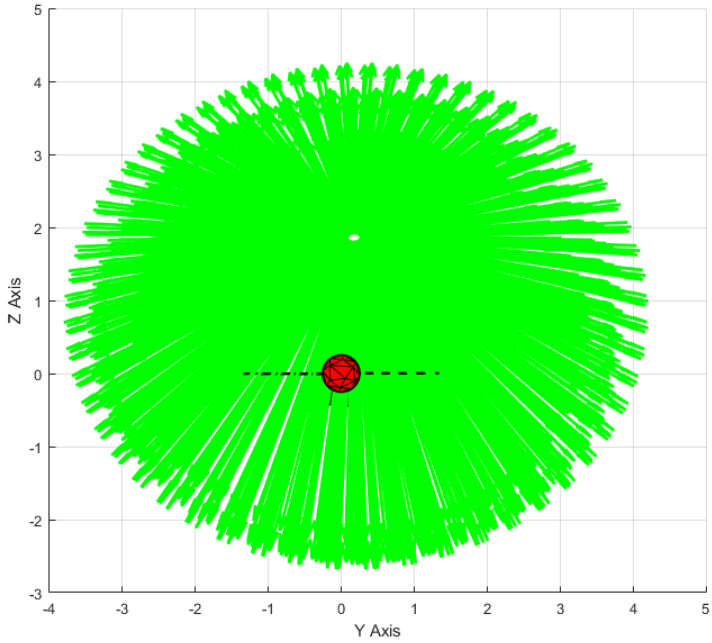

Figure 3.9: Scattering of All Fragments at Detonation Point 12 on YZ Axis for the 1^{st} Scenario

Since the detonation analysis is performed at 0.25 m intervals, including the moment the missile detects the target, it means that the missile travels 2.75 meters after detecting the target at the detonation point 12.

$$dist = (\det_{no} - 1) * (\det_{interval}) \tag{3.5}$$

$$dist = (12 - 1) * 0.25 = 2.75m \tag{3.6}$$

In this scenario, since the relative speed of the missile to target is ~ 886 m / s, when the missile's warhead is detonated ~3.1 milliseconds after detecting the target, most fragments will have hit the target.

$$rel_{speed} = \sqrt{(misvel_x - t\arg vel_x)^2 + (misvel_y - t\arg vel_y)^2 + (misvel_z - t\arg vel_z)^2} \tag{3.7}$$

$$delay_{time} = \frac{dist}{|rel_{vel}|} \tag{3.8}$$

$$delay_{time} = \frac{2.75}{886} = \sim 3.1ms \tag{3.9}$$

The number of fragments hitting the target for all detonation points with respect to delay time can be seen in Figure 3.10. Time is started from the first detonation point.

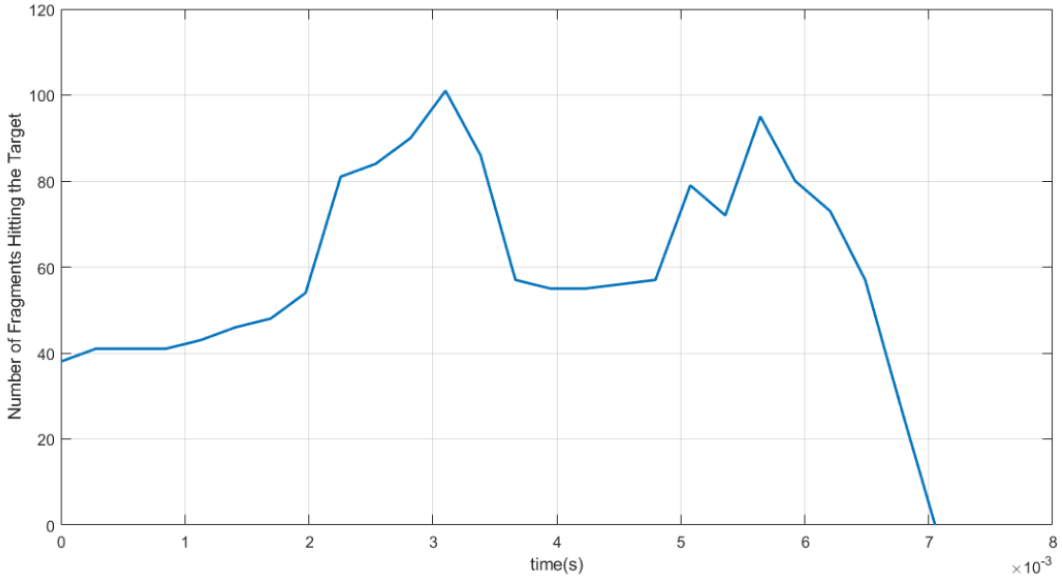

Figure 3.10: The Number of Fragments Hitting The Target vs Time for the 1^{st} Scenario

3.2.2 The Second Scenario

The second scenario is chosen as a fighter arriving at an altitude of 5000 meters and a speed of 250 m/s.

In the second scenario, the missile and target speed, Euler angles, AOA, and sideslip angle at the time of engagement are in Table 3.3.

Table 3.3: Missile and Target Kinematics for the 2^{nd} Scenario

	Missile	**Target**
Speed	512.3 m/s	250 m/s
Roll Angle (ϕ)	0.88 °	0
Pitch Angle (θ)	32.37 °	0
Yaw Angle (ψ)	4.65 °	180 °
AOA (α)	9.74 °	0
Sideslip Angle(β)	0.03 °	0

In this scenario, the target is detected by the missile while the missile is ~ 10.87 meters away from the target.

Using Eqn. (3.1), the total distance at which the analyses are carried out is calculated as 21.74 meters.

The kill analysis is carried out at every 0.25 m along the 21.74 meters road, including when the missile detected the target. Thus, the total number of detonation points is calculated as 88.

For the second scenario, the number of fragments striking the target at each detonation point is shown in Table 3.4.

Table 3.4: Detonation Point vs Number of Fragments Hitting the Target for the 2^{nd} Scenario

Detonation Point	**1**	**2**	**3**	**4**	**5**	**6**	**7**	**8**	**9**	**10**	**11**	**12**	**13**	**14**	**15**	**16**	**17**	**18**	**19**	**20**	**21**	**22**
No. of Fragments Hitting the Target	31	37	42	44	46	49	50	51	54	56	59	61	63	65	68	73	80	83	88	90	96	104
Detonation Point	**23**	**24**	**25**	**26**	**27**	**28**	**29**	**30**	**31**	**32**	**33**	**34**	**35**	**36**	**37**	**38**	**39**	**40**	**41**	**42**	**43**	**44**
No. of Fragments Hitting the Target	109	117	121	128	137	140	145	152	170	190	213	222	227	242	269	298	329	357	372	390	410	426
Detonation Point	**45**	**46**	**47**	**48**	**49**	**50**	**51**	**52**	**53**	**54**	**55**	**56**	**57**	**58**	**59**	**60**	**61**	**62**	**63**	**64**	**65**	**66**
No. of Fragments Hitting the Target	439	444	452	450	452	451	446	443	438	435	430	417	411	402	386	389	394	409	425	445	459	473
Detonation Point	**67**	**68**	**69**	**70**	**71**	**72**	**73**	**74**	**75**	**76**	**77**	**78**	**79**	**80**	**81**	**82**	**83**	**84**	**85**	**86**	**87**	**88**
No. of Fragments Hitting the Target	486	493	492	486	467	442	435	436	461	507	442	127	126	112	66	14	0	0	0	0	0	0

Fragments hitting the target at each detonation point can be seen from Figure 3.11, Figure 3.12, and Figure 3.13. Each detonation point is shown in a different colour. The first detonation point starts from the fighter's nose, and the other detonation points are shown on the relative velocity vector for 21.74 meters at 0.25 m intervals.

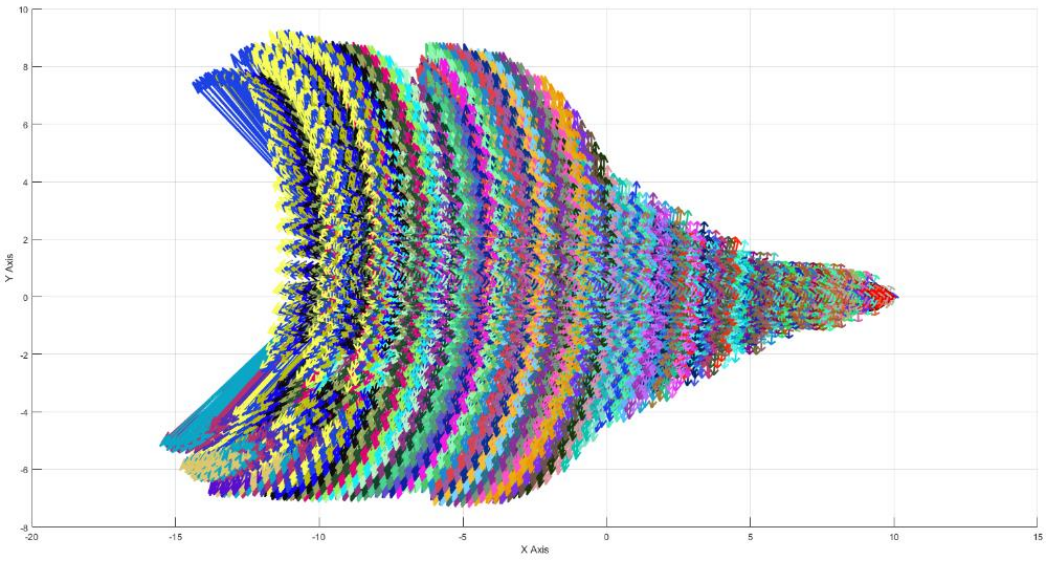

Figure 3.11: Scattering of Striking Fragments at All Detonation Points on XY Axis for the 2^{nd} Scenario

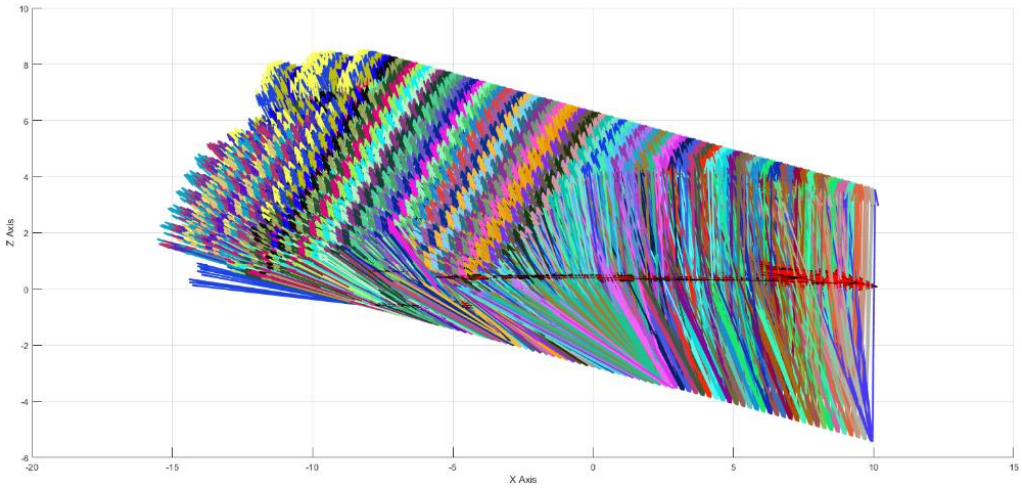

Figure 3.12: Scattering of Striking Fragments at All Detonation Points on XZ Axis for the 2^{nd} Scenario

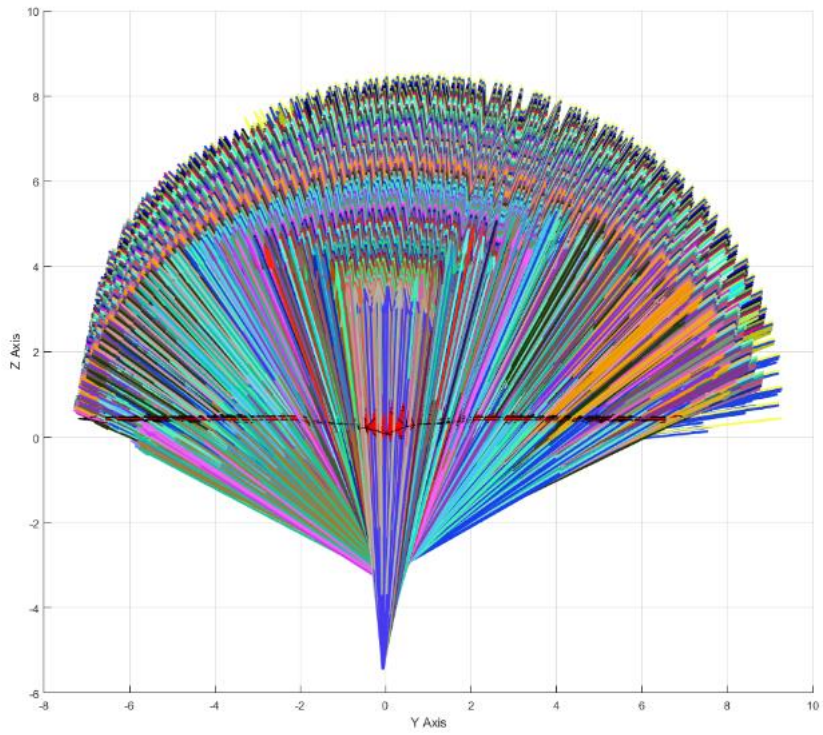

Figure 3.13: Scattering of Striking Fragments at All Detonation Points on YZ Axis for the 2^{nd} Scenario

As can be seen from Table 3.4, the target is hit mostly by the fragment at the detonation point 76.

The scattering plot of the fragments hitting the target at the seventy-sixth detonation point can be seen in Figure 3.14, Figure 3.15, and Figure 3.16.

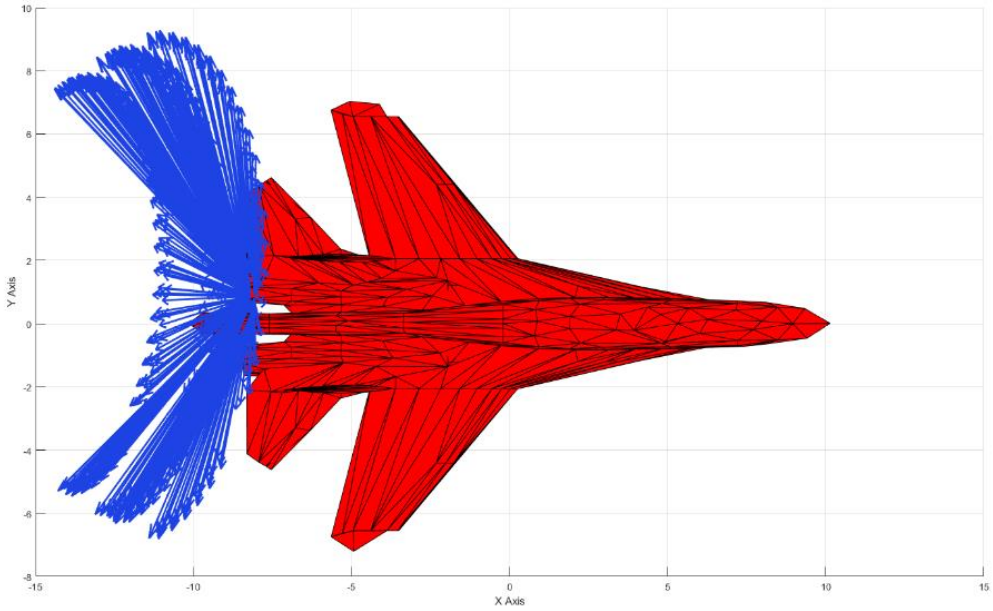

Figure 3.14: Scattering of Striking Fragments at Detonation Point 76 on XY Axis for the 2^{nd} Scenario

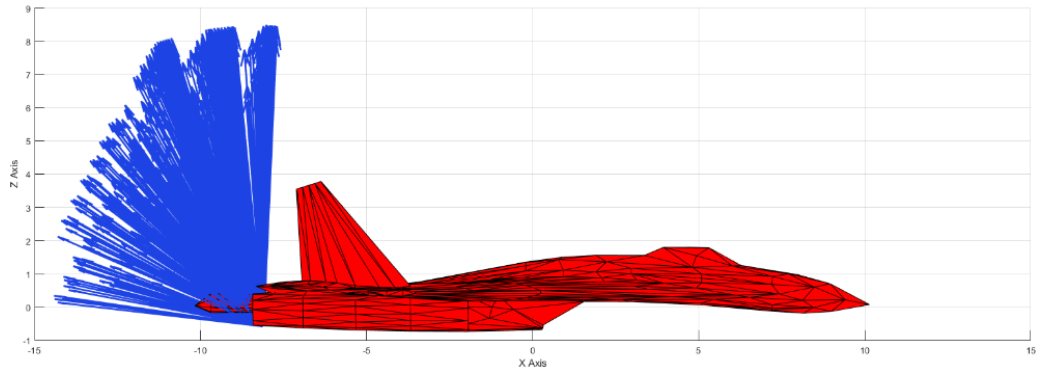

Figure 3.15: Scattering of Striking Fragments at Detonation Point 76 on XZ Axis for the 2^{nd} Scenario

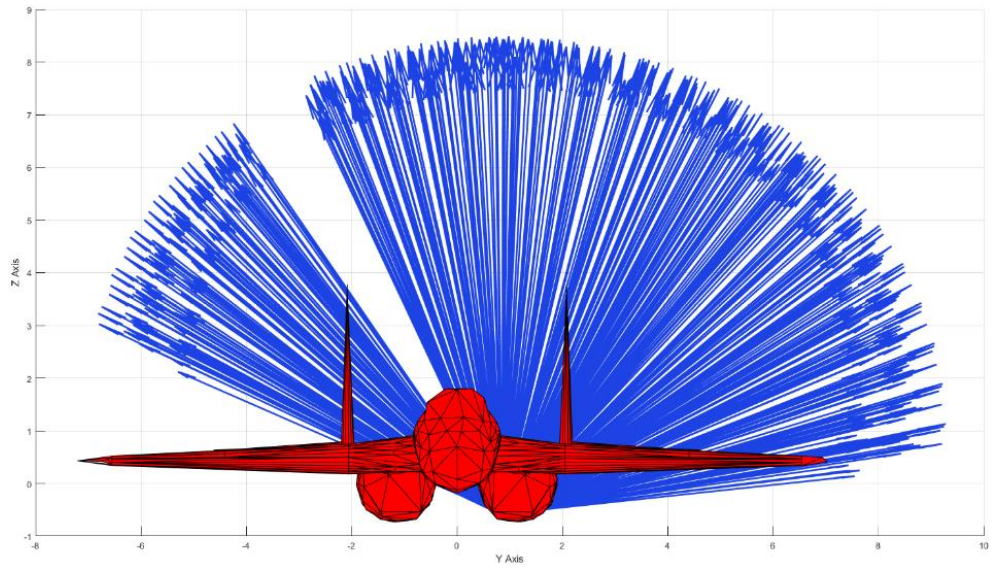

Figure 3.16: Scattering of Striking Fragments at Detonation Point 76 on YZ Axis for the 2^{nd} Scenario

The scattering plot of all fragments, including fragments non-hitting the target at the seventy-sixth detonation point can be seen from Figure 3.17, Figure 3.18, and Figure 3.19.

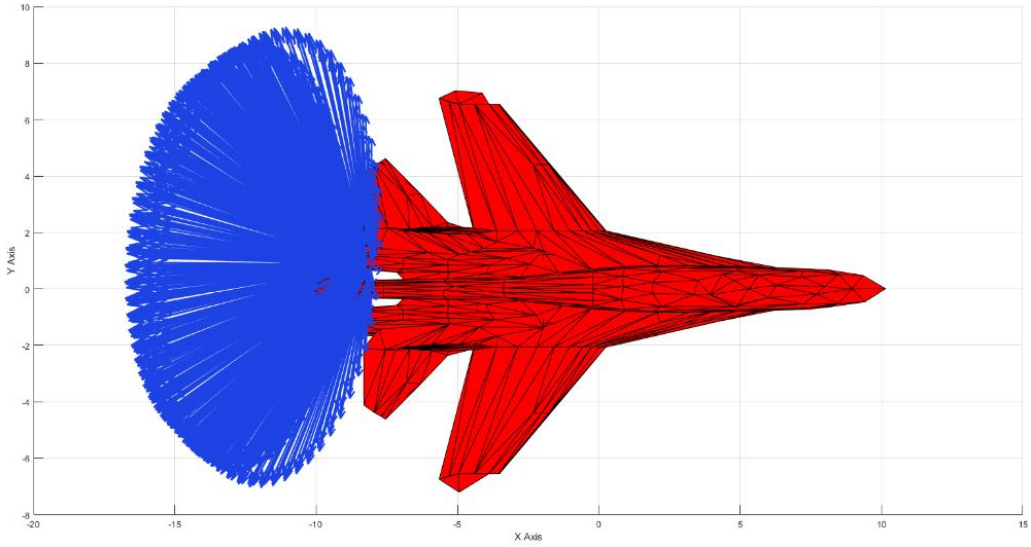

Figure 3.17: Scattering of All Fragments at Detonation Point 76 on XY Axis for the 2^{nd} Scenario

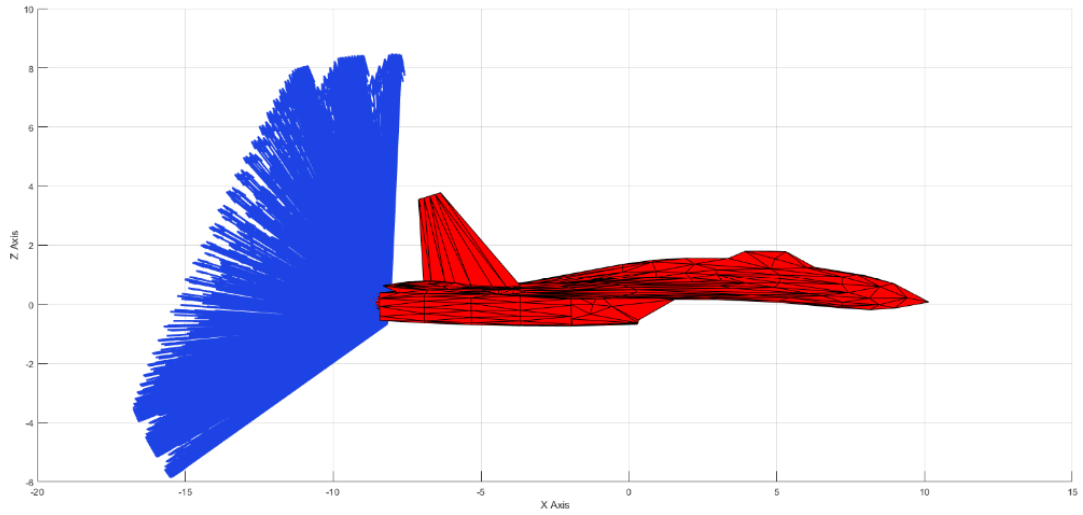

Figure 3.18: Scattering of All Fragments at Detonation Point 76 on XZ Axis for the 2^{nd} Scenario

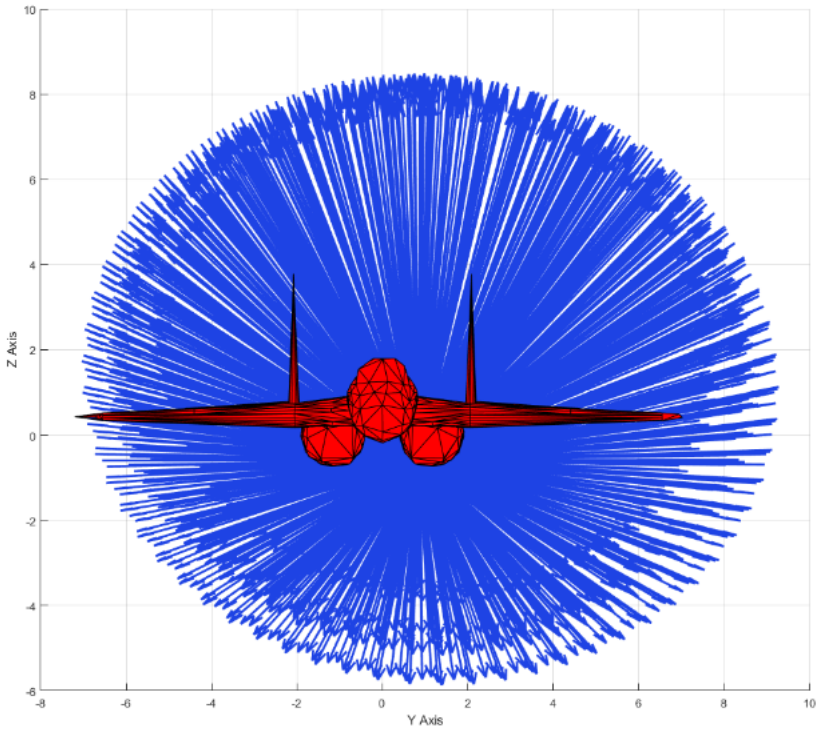

Figure 3.19: Scattering of All Fragments at Detonation Point 76 on YZ Axis for the 2^{nd} Scenario

Since the detonation analysis is performed at 0.25 m intervals, including the moment the missile detects the target, it means that the missile travels 18.75 meters after detecting the target at the detonation point 76.

In this scenario, since the relative speed of the missile to the target is ~ 748.77 m / s, when the missile's warhead is detonated ~25 milliseconds after detecting the target, most fragments will have hit the target.

The number of fragments hitting the target for all detonation points with respect to delay time can be seen in Figure 3.20. Time is started from the first detonation point.

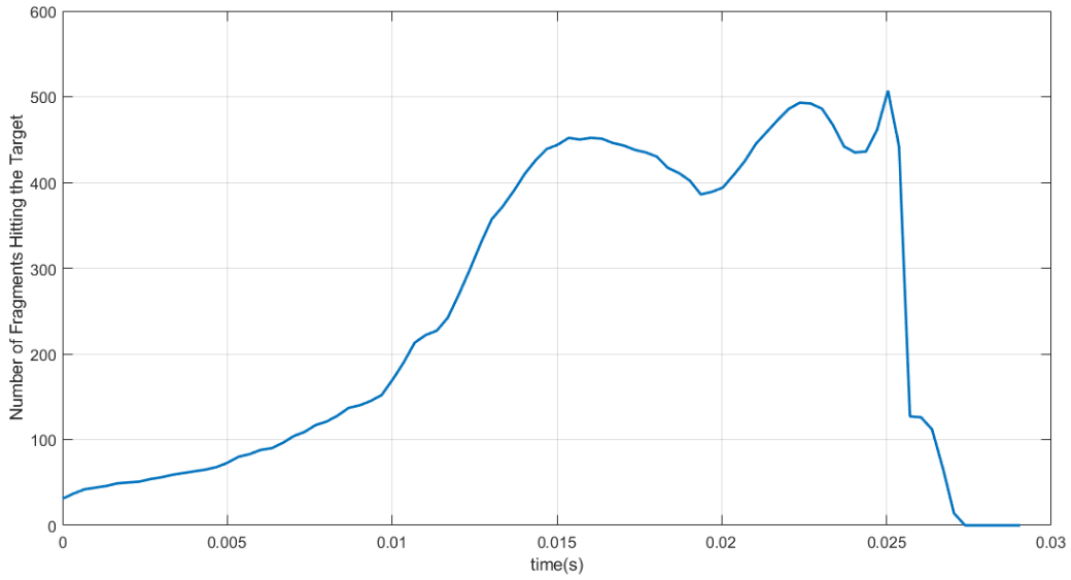

Figure 3.20: The Number of Fragments Hitting The Target vs Time for the 2^{nd} Scenario

When the results of the kill analysis of the scenario 1 and 2 are examined, it is seen that the analysis distance is longer in the second scenario because the missile detects the target earlier than the first scenario. The longer detection distance in the

second scenario may be because the second target's size is larger than the first target.

In addition, in the first scenario, since the target comes from a low altitude, it is hit by the missile by diving. Therefore, the warhead appears to be exploding above the target.

In cases where a fragment hits more than one triangle at the same detonation point, that fragment is counted as hitting the triangle closest to it. Since the fragment's first position and the point where the fragment intersects the triangle is known, the distance between these two points is calculated for all the triangles the fragment hits.

3.2.3 Scenarios with the Different Miss Distances

The first scenario is analyzed for 14 different miss distance values, with all other parameters remaining the same. These fourteen scenarios are achieved by changing the z-component value of the original miss distance in the first scenario. In this way, the effect of the change in altitude between the missile and the target in the terminal condition on the results can be observed.

The fourteen scenarios' kill analysis results, and the first scenario's actual result can be seen in Table 3.5. The maximum number of fragments hitting the target is shown in thick outside borders in Table 3.5.

Table 3.5: Number of Fragments Hitting the Target for Scenarios with Different Miss Distances

Scenarios:		1 (Original Value)	2	3	4	5	6	7	8	9	10	11	12	13	14	15
Miss Distance:		2.18317	3.11754	4.08312	5.06208	6.04793	7.03777	8.03013	9.02418	10.01941	11.01551	12.01225	13.00950	14.00714	15.00509	16.00329
Detonation Point	1	38	29	21	24	18	17	18	22	17	8	6	6	8	6	1
	2	41	29	21	38	18	17	22	20	14	6	6	7	7	5	0
	3	41	29	22	24	18	24	20	20	10	6	6	7	6	6	0
	4	41	30	41	19	19	25	24	15	9	6	8	6	7	8	0
	5	43	30	40	19	28	24	15	14	9	6	8	8	8	7	0
	6	46	37	23	24	31	20	15	12	9	9	10	7	8	6	0
	7	48	66	23	37	24	20	15	10	11	9	8	9	6	3	0
	8	54	38	38	35	18	17	14	12	17	10	8	6	4	2	0
	9	81	37	50	19	24	18	16	17	11	7	6	4	2	2	0
	10	84	73	28	19	22	24	12	10	9	6	6	3	2	2	0
	11	90	48	24	34	26	14	14	10	11	6	4	2	2	2	0
	12	101	44	42	32	19	12	11	11	9	4	2	2	2	3	0
	13	86	53	24	21	17	12	11	10	8	2	2	2	3	2	0
	14	57	36	33	20	16	13	10	9	5	2	3	3	2	3	0
	15	55	37	29	19	14	13	9	6	4	3	3	2	3	2	0
	16	55	39	27	24	15	12	8	4	4	3	3	2	2	2	0
	17	56	52	30	21	13	10	4	4	3	4	2	2	2	1	0
	18	57	36	38	13	12	7	4	4	3	4	2	1	0	0	0
	19	79	50	20	16	11	5	4	4	4	3	1	0	0	0	0
	20	72	48	20	18	5	4	4	4	3	1	0	0	0	0	0
	21	95	43	26	8	4	4	4	2	0	0	0	0	0	0	0
	22	80	29	15	4	4	3	1	0	0	0	0	0	0	0	0
	23	73	25	6	4	2	0	0	0	0	0	0	0	0	0	0
	24	57	8	6	1	0	0	0	0	0	0	0	0	0	0	0
	25	28	7	0	0	0	0	0	0	0	0	0	0	0	0	0
	26	0	0	0	0	0	0	0	0	0	0	0	0	0	0	0
Total Fragment Number Hitting the Target:		1558	953	647	493	378	315	255	220	170	105	94	79	74	62	1

The maximum number of fragments hitting the target with respect to miss distance can be seen in Figure 3.21.

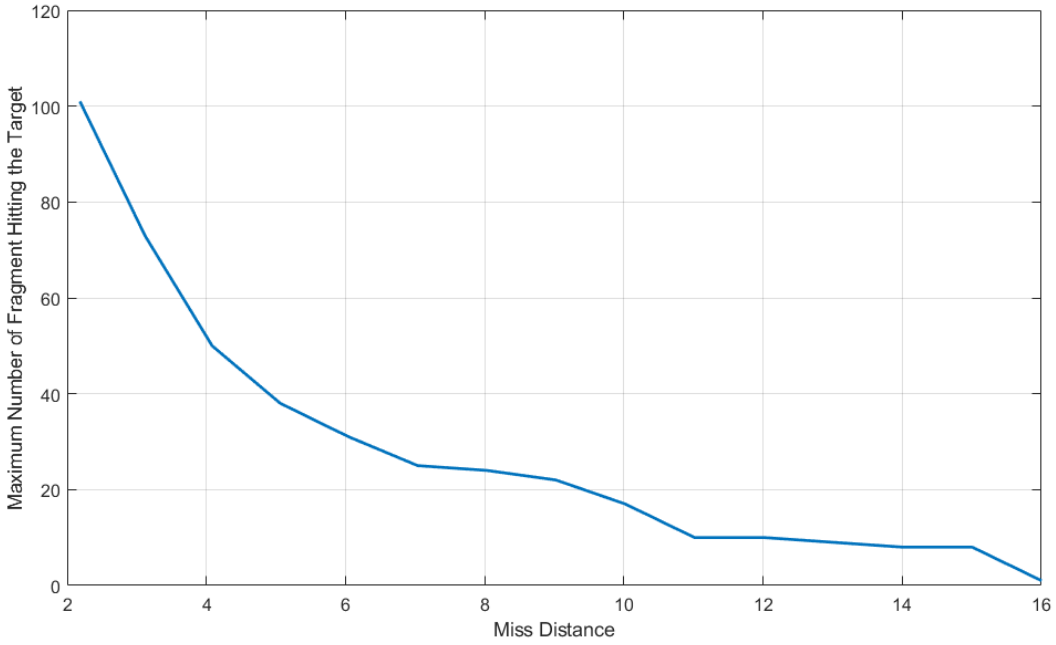

Figure 3.21: Maximum Number of Fragment Hitting the Target vs Miss Distance

When the results are examined, it is observed that the number of striking fragments to the target decreases when the miss distance is increased as an altitude.

3.2.4 Scenarios with the Warhead Uncertainties

Monte Carlo analysis is performed for the first scenario to examine the effect of uncertainties added to segment limits and fragment speeds on the results. Segment limit uncertainty is distributed uniformly between -2 and +2 degrees, and fragment speed uncertainty is distributed uniformly between -20 and +20 m/s. The Monte Carlo run number is chosen as fifty. Then, segment limit uncertainties are added to real segment limits in Eqn. (2.8) except for 90° segment limit, and fragment speed uncertainties are added to real fragment speeds in Eqn. (2.7). Fragments in front of the 90° segment limit are scattered forward, and fragments behind the 90° segment limit are scattered to the back. In order not to break this logic, uncertainty is not added to the 90° segment limit.

Segment limit and fragment speed values used in the Monte Carlo analysis are as in Table 3.6 and Table 3.7.

Table 3.6: Segment Limits Used in the Monte Carlo Analysis

Monte Carlo Number	Segment Limits (deg)				
1	81,16182	85,28456	90,00000	88,70323	87,08937
2	78,68959	86,80316	90,00000	89,47884	85,74774
3	80,74290	83,69767	90,00000	88,68897	84,22142
4	81,88354	85,07000	90,00000	87,08236	84,81267
5	78,81632	84,70249	90,00000	88,73011	86,78887
6	78,87851	86,38861	90,00000	88,60884	87,80995
7	79,75282	86,49906	90,00000	89,33867	87,79169
8	78,12040	86,27936	90,00000	87,69462	84,92625
9	79,04384	84,57194	90,00000	89,54447	85,81521
10	79,10044	83,85516	90,00000	87,47260	86,60857
11	79,45745	83,56510	90,00000	87,98359	86,70315
12	78,34022	84,60048	90,00000	86,66298	84,74754
13	81,13939	85,52696	90,00000	88,61438	84,37643
14	81,48678	83,86925	90,00000	87,12891	85,09740
15	81,04755	85,47892	90,00000	86,88191	86,83370
16	79,03098	83,67033	90,00000	88,30909	86,51049
17	81,08811	84,14004	90,00000	88,86671	87,44750
18	79,34403	85,88743	90,00000	87,19201	86,72669
19	78,94692	85,39423	90,00000	89,39194	84,60564
20	79,88872	85,45219	90,00000	89,18134	87,08573
21	81,53073	86,74435	90,00000	88,03014	87,62948
22	78,79000	84,11082	90,00000	89,71406	86,84790
23	79,42872	85,35894	90,00000	89,44890	86,44544
24	80,67065	86,35504	90,00000	87,46649	86,09465
25	78,53256	86,84101	90,00000	89,11155	87,32176
26	81,42440	83,50461	90,00000	87,60966	85,40664
27	81,49035	85,81477	90,00000	89,76040	86,63258
28	81,82272	85,53411	90,00000	88,49660	86,94423
29	80,07212	86,57552	90,00000	86,66617	84,05632
30	80,61480	85,34294	90,00000	89,69378	84,00464
31	79,26830	86,75065	90,00000	87,91581	87,64725
32	80,17685	85,09565	90,00000	88,97254	85,89253
33	81,43505	84,56579	90,00000	88,16542	85,69588
34	78,21244	83,82503	90,00000	88,20911	86,14043
35	79,64017	83,04312	90,00000	88,33311	86,25243
36	80,46767	85,81681	90,00000	86,25048	86,11578
37	78,58296	85,12457	90,00000	87,87728	85,39847
38	79,65505	86,46535	90,00000	87,90110	84,35512
39	80,98080	86,08348	90,00000	88,22244	84,17703
40	79,69745	86,44601	90,00000	87,25401	84,06214
41	80,10906	83,30567	90,00000	87,23507	84,66636
42	80,67608	84,24354	90,00000	87,53018	86,82170
43	79,42437	84,04184	90,00000	89,42041	87,15553
44	80,43920	86,56204	90,00000	89,41830	86,57539
45	80,79809	86,38314	90,00000	86,18806	85,01024
46	78,50857	85,41826	90,00000	86,21431	84,29686
47	81,45816	83,66310	90,00000	88,67905	84,59792
48	79,13167	86,32755	90,00000	88,93144	85,00913
49	78,95359	85,03366	90,00000	88,31606	87,75699
50	80,57929	86,68557	90,00000	87,97188	85,26140

Table 3.7: Fragment Speeds Used in the Monte Carlo Analysis

Monte Carlo Number	Fragment Speeds(m/s)			
1	890,92289	1084,72368	1096,85092	1286,98879
2	884,24172	1094,49425	1099,53009	1319,74507
3	907,04261	1091,43213	1095,63968	1305,19554
4	886,98152	1087,82181	1087,99397	1312,69018
5	915,48415	1101,86228	1107,77929	1319,80037
6	891,63011	1081,41832	1098,28307	1300,37790
7	891,97621	1099,49412	1103,50895	1291,06138
8	911,22424	1106,32209	1102,90784	1316,30440
9	882,85076	1106,07857	1086,90901	1294,48536
10	895,76178	1102,60488	1104,95295	1316,55373
11	902,93913	1092,25680	1080,46401	1282,27317
12	888,14552	1100,09963	1089,00463	1301,43426
13	909,73565	1117,70648	1103,22422	1280,03346
14	893,72831	1098,59851	1090,82610	1287,42464
15	889,82911	1085,91415	1098,00726	1315,78152
16	900,46093	1119,11237	1085,05032	1289,85302
17	911,95278	1119,58209	1100,87355	1299,82331
18	885,08806	1083,10141	1080,56966	1290,80792
19	899,62095	1108,15606	1084,02812	1310,93552
20	897,48364	1099,50523	1094,70686	1287,00129
21	880,10455	1105,97429	1118,21836	1284,67520
22	890,35562	1106,78140	1110,77753	1305,26893
23	898,01803	1080,09432	1104,11157	1298,93005
24	910,65970	1109,42794	1104,92838	1294,88030
25	918,84039	1087,92147	1109,34636	1306,87421
26	893,34600	1104,44986	1096,60707	1291,36012
27	907,91007	1092,55079	1116,88087	1289,08735
28	880,98657	1084,97317	1086,82155	1295,27558
29	918,11801	1119,48948	1098,40698	1317,41284
30	888,02646	1082,03372	1112,49528	1312,17160
31	891,17332	1113,21255	1119,47646	1318,56491
32	913,24794	1109,15858	1081,00035	1317,76202
33	915,66350	1114,67557	1101,42897	1313,73544
34	888,04880	1097,02109	1083,34965	1285,34188
35	897,82610	1087,70359	1104,01374	1284,65233
36	915,39651	1099,18470	1083,37962	1282,49202
37	901,19276	1094,26275	1099,83335	1282,35061
38	910,53910	1112,33464	1110,48622	1282,09729
39	894,73861	1089,94991	1112,21386	1309,32107
40	883,71305	1102,33798	1094,37873	1293,87807
41	884,26388	1108,96402	1083,69200	1308,44043
42	900,42786	1085,95359	1102,15011	1308,04587
43	907,32599	1110,71591	1118,16706	1308,26702
44	910,13444	1095,72814	1083,49280	1307,88318
45	900,44428	1117,50474	1116,65479	1310,20528
46	895,48023	1106,67440	1092,44096	1299,87984
47	884,89706	1110,61573	1100,85534	1285,34673
48	888,50239	1113,82639	1082,30058	1294,99897
49	887,42404	1092,92388	1089,51477	1295,13224
50	903,78158	1112,21322	1095,04069	1280,96284

The Monte Carlo analysis results are shown in Table 3.8, Table 3.9, Table 3.10, Table 3.11, and Table 3.12. The maximum number of fragments hitting the target is shown in thick outside borders in these tables.

Table 3.8: The Monte Carlo Analysis Results from the Run Number 1 to 10

		Run Number									
		1	**2**	**3**	**4**	**5**	**6**	**7**	**8**	**9**	**10**
Detonation Point	**1**	39	38	40	37	38	39	39	38	38	39
	2	41	40	41	41	41	41	40	41	41	41
	3	41	41	41	41	41	41	41	41	41	41
	4	41	41	41	41	41	41	41	41	41	41
	5	43	43	44	43	43	43	43	43	43	43
	6	47	46	46	45	46	47	46	45	46	46
	7	47	48	47	46	48	48	48	48	49	49
	8	54	55	53	55	54	55	55	55	58	57
	9	80	85	81	80	80	84	81	81	89	87
	10	82	77	86	84	85	81	80	82	75	79
	11	95	89	98	95	92	96	89	83	93	93
	12	98	103	93	96	101	100	106	106	103	96
	13	86	83	82	80	87	87	86	80	85	86
	14	54	62	63	66	58	55	54	66	58	60
	15	55	55	55	55	55	55	55	55	55	55
	16	55	55	55	55	55	55	55	55	55	55
	17	56	56	56	56	56	56	56	56	56	56
	18	58	57	57	57	58	57	58	56	59	57
	19	78	82	78	80	79	82	80	81	86	84
	20	75	66	77	76	72	68	68	71	66	71
	21	95	100	94	96	97	97	98	98	96	93
	22	83	82	82	80	81	83	83	80	84	81
	23	74	73	74	73	73	74	74	73	74	73
	24	56	55	57	54	57	56	56	58	52	52
	25	27	27	27	27	29	27	29	30	27	28
	26	0	0	2	2	0	0	0	2	0	0
Total Fragment Number Hitting the Target:		1560	1559	1570	1561	1567	1568	1561	1565	1570	1563

Table 3.9: The Monte Carlo Analysis Results from the Run Number 11 to 20

		Run Number									
		11	**12**	**13**	**14**	**15**	**16**	**17**	**18**	**19**	**20**
Detonation Point	**1**	41	37	38	39	38	40	40	39	38	39
	2	41	41	41	41	41	41	41	41	41	41
	3	41	41	41	41	41	41	41	41	41	41
	4	41	41	41	41	41	42	41	41	41	41
	5	45	43	43	43	43	43	43	43	43	43
	6	47	46	46	45	45	46	47	47	46	47
	7	49	48	46	47	48	49	47	48	47	48
	8	56	58	52	56	54	57	52	57	55	54
	9	86	88	73	80	80	87	77	88	82	82
	10	82	76	89	82	82	80	89	79	79	83
	11	100	93	86	96	94	91	90	96	92	92
	12	93	99	109	96	98	102	104	99	103	102
	13	86	81	83	85	88	87	86	88	81	86
	14	55	65	59	59	63	55	54	55	64	54
	15	55	55	55	55	55	55	55	55	55	55
	16	55	55	55	55	55	55	55	55	55	55
	17	56	56	56	56	56	56	56	56	56	56
	18	58	57	57	57	57	58	59	56	58	59
	19	83	85	74	80	78	84	76	83	82	81
	20	74	68	71	77	74	69	73	69	68	71
	21	93	97	99	94	94	96	97	95	98	97
	22	85	80	81	81	81	84	83	83	84	83
	23	74	73	74	72	73	74	74	73	74	74
	24	53	52	61	53	55	52	58	55	56	56
	25	26	28	32	27	27	29	30	27	28	27
	26	0	0	0	0	0	0	0	0	2	0
Total Fragment Number Hitting the Target:		1575	1563	1562	1558	1561	1573	1568	1569	1569	1567

Table 3.10: The Monte Carlo Analysis Results from the Run Number 21 to 30

		Run Number									
		21	**22**	**23**	**24**	**25**	**26**	**27**	**28**	**29**	**30**
Detonation Point	**1**	39	40	39	38	39	39	39	39	36	38
	2	40	41	41	40	40	41	41	41	40	41
	3	41	41	41	41	41	41	41	41	41	41
	4	41	42	41	41	41	41	41	41	41	41
	5	42	43	43	42	42	43	42	43	42	43
	6	46	47	46	45	46	46	46	47	44	46
	7	47	49	48	48	48	47	47	47	47	47
	8	54	58	55	52	52	56	52	56	52	56
	9	82	88	82	73	75	80	71	82	70	85
	10	80	76	82	88	85	83	92	82	88	81
	11	81	93	98	82	89	94	91	97	79	98
	12	111	102	95	109	104	96	104	98	111	97
	13	86	86	86	88	86	86	86	86	76	80
	14	54	57	57	56	55	59	54	54	71	64
	15	55	55	55	55	55	55	55	55	55	55
	16	55	55	55	55	55	55	55	55	55	55
	17	56	56	56	56	56	56	56	56	56	56
	18	56	59	59	57	57	57	59	58	56	58
	19	78	86	81	76	78	81	74	80	77	82
	20	67	68	75	70	72	75	74	74	70	75
	21	97	96	93	97	98	94	97	94	100	96
	22	83	82	82	81	82	81	82	83	77	80
	23	74	74	74	73	74	73	75	74	75	74
	24	56	52	56	61	60	52	61	53	61	55
	25	33	29	27	32	29	28	29	26	34	28
	26	0	0	0	0	0	0	0	0	4	3
Total Fragment Number Hitting the Target:		1554	1575	1567	1556	1559	1559	1564	1562	1558	1575

Table 3.11: The Monte Carlo Analysis Results from the Run Number 31 to 40

		Run Number									
		31	**32**	**33**	**34**	**35**	**36**	**37**	**38**	**39**	**40**
Detonation Point	**1**	39	38	38	40	41	39	38	38	38	38
	2	40	41	41	41	41	41	41	40	41	40
	3	41	41	41	41	41	41	41	41	41	41
	4	41	41	41	42	42	41	41	41	41	41
	5	43	43	43	43	45	43	43	42	43	43
	6	46	46	46	47	46	45	46	44	45	44
	7	48	48	47	49	49	48	49	47	47	47
	8	55	52	52	58	57	52	55	52	54	55
	9	84	77	71	90	84	72	84	75	78	85
	10	80	86	91	75	81	89	82	85	83	77
	11	80	93	88	99	99	91	93	82	90	84
	12	114	101	103	96	93	102	100	112	103	106
	13	88	84	84	87	86	88	87	83	80	81
	14	55	61	61	57	55	54	58	60	63	64
	15	55	55	55	55	55	55	55	55	55	55
	16	55	55	55	55	55	55	55	55	55	55
	17	56	56	56	56	56	56	56	56	56	56
	18	56	58	58	57	58	57	57	55	56	56
	19	81	78	74	85	83	76	82	77	77	81
	20	65	72	74	67	75	72	71	70	73	66
	21	98	99	98	94	92	97	95	98	97	99
	22	82	85	80	85	83	83	81	82	80	80
	23	73	73	73	74	74	73	73	73	73	74
	24	56	59	61	51	52	61	55	59	57	55
	25	35	28	30	26	27	28	27	34	29	29
	26	0	0	0	0	0	0	0	0	2	2
Total Fragment Number Hitting the Target:		1566	1570	1561	1570	1570	1559	1565	1556	1557	1554

Table 3.12: The Monte Carlo Analysis Results from the Run Number 41 to 50

		Run Number									
		41	**42**	**43**	**44**	**45**	**46**	**47**	**48**	**49**	**50**
Detonation Point	**1**	39	40	40	38	37	36	39	38	39	38
	2	41	41	41	40	40	41	41	40	41	40
	3	41	41	41	41	41	41	41	41	41	41
	4	42	41	41	41	41	41	41	41	41	41
	5	44	43	43	42	42	43	43	43	43	42
	6	45	46	47	45	44	46	46	45	47	45
	7	48	48	49	48	48	48	47	48	49	48
	8	58	54	54	52	52	55	56	55	58	52
	9	89	79	82	73	76	83	85	84	87	76
	10	78	84	83	88	84	76	81	78	76	86
	11	94	97	90	92	80	88	92	86	95	82
	12	96	95	105	103	112	102	101	110	98	111
	13	80	88	86	87	78	78	83	83	87	86
	14	66	56	55	56	68	68	59	60	55	57
	15	55	55	55	55	55	55	55	55	55	55
	16	55	55	55	55	55	55	55	55	55	55
	17	56	56	56	56	56	56	56	56	56	56
	18	57	57	59	59	55	57	57	56	58	56
	19	85	78	80	76	75	82	82	82	86	76
	20	67	77	72	71	68	67	72	63	69	69
	21	95	92	96	98	99	97	97	100	96	98
	22	82	80	82	85	82	80	82	84	83	82
	23	73	73	74	74	73	73	74	74	74	74
	24	51	57	56	61	58	55	52	55	52	60
	25	28	27	29	27	36	29	28	32	26	33
	26	2	0	0	0	1	2	0	0	0	0
Total Fragment Number Hitting the Target:		1567	1560	1571	1563	1556	1554	1565	1564	1567	1559

The graph of the number of fragments hitting the target according to the detonation point for 50 runs is shown in Figure 3.22.

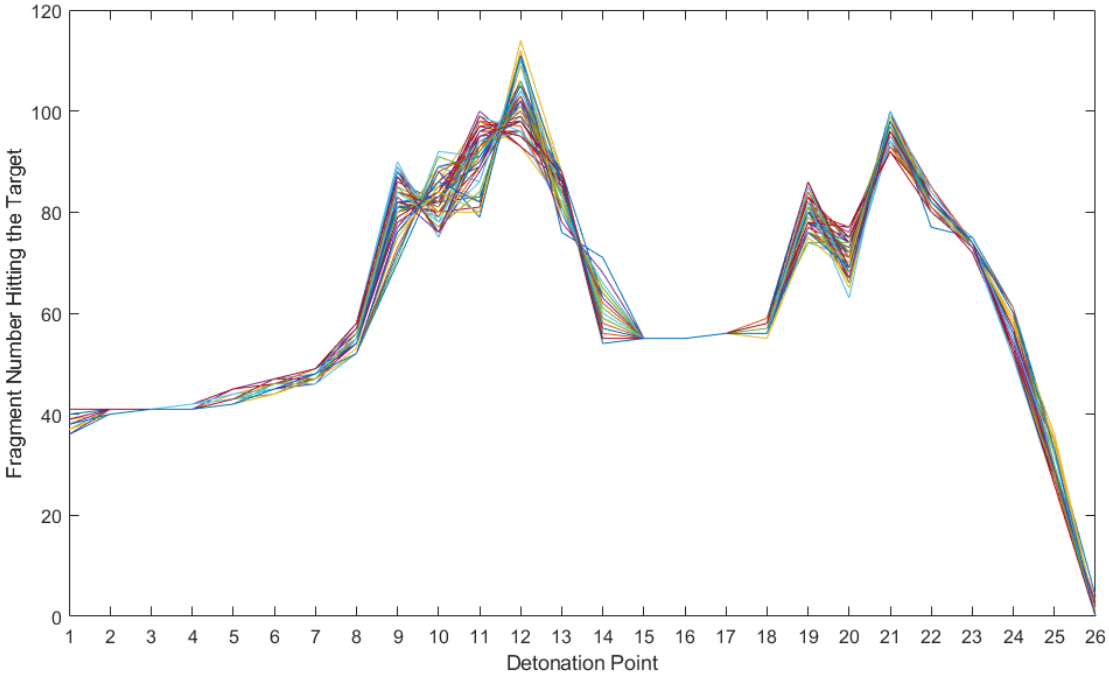

Figure 3.22: Fragment Number Hitting the Target vs Detonation Point for 50 Runs

When the analysis results are examined, in 42 out of 50 runs, the most particles hit the target at the detonation point 12, like the first scenario. The maximum number of fragments hitting the target in only eight runs is at detonation point 11. The detonation point 11 is not far from detonation point 12. As a result, the uncertainties added to the fragment speed and the segment limit do not dramatically affect the kill analysis tool results.

3.2.5 Result Comparison with the Another Tool

The tool developed in the thesis is compared with another tool that calculates the number of fragments hitting the target when the warhead is detonated. In the method used by another tool, spheres in the target's diameter are placed along the target's body. The distance of the fragments from the sphere's center is checked, and if this distance is smaller than the sphere's radius, it is considered to have hit the target. The placement of the spheres on the cruise missile can be seen in Figure

3.23 and Figure 3.24. In the continuation of the thesis, this tool is named a sphere tool.

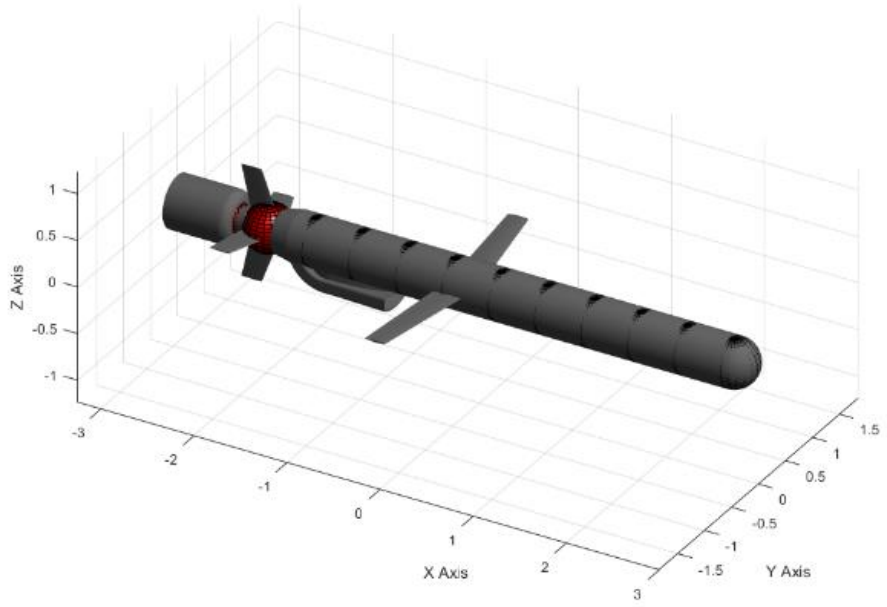

Figure 3.23: Placement of the Spheres on the Cruise Missile

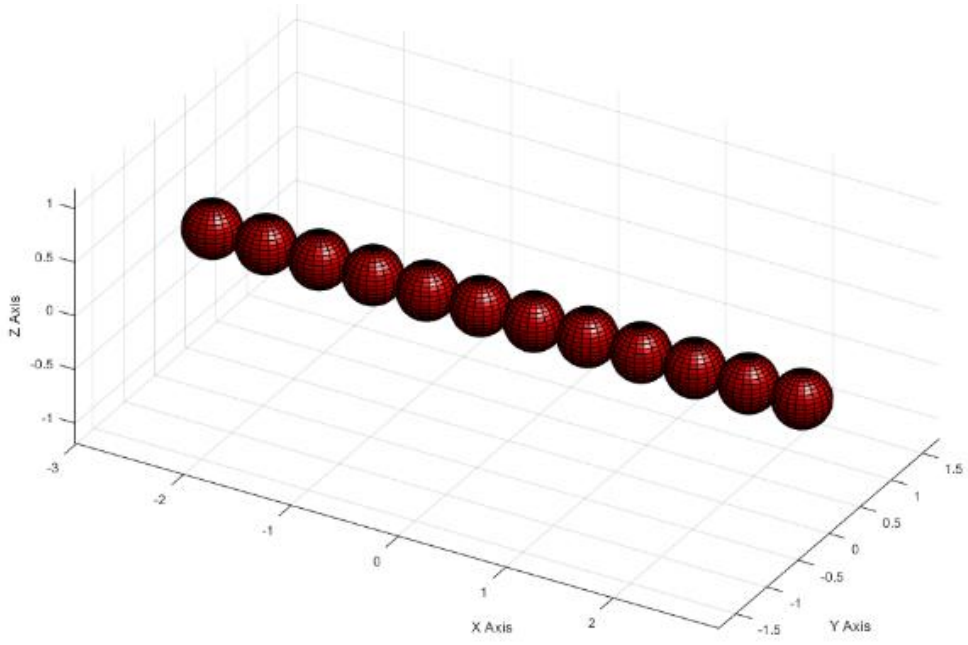

Figure 3.24: Appearances of the Spheres

The kill analysis is performed for the first scenario in the sphere tool, and the results in Table 3.13 are obtained.

Table 3.13: Number of Fragments Hitting the Target Using the Sphere Tool

Detonation Point	**1**	**2**	**3**	**4**	**5**	**6**	**7**	**8**	**9**	**10**	**11**	**12**	**13**
No. of Fragments Hitting the Target	33	26	35	30	33	33	31	37	31	43	32	48	36
Detonation Point	**14**	**15**	**16**	**17**	**18**	**19**	**20**	**21**	**22**	**23**	**24**	**25**	**26**
No. of Fragments Hitting the Target	50	40	46	45	45	48	45	54	55	39	14	0	0

Fragments hitting the target calculated with the sphere tool at each detonation point can be seen from Figure 3.25, Figure 3.26, and Figure 3.27. Each detonation point is shown in a different colour.

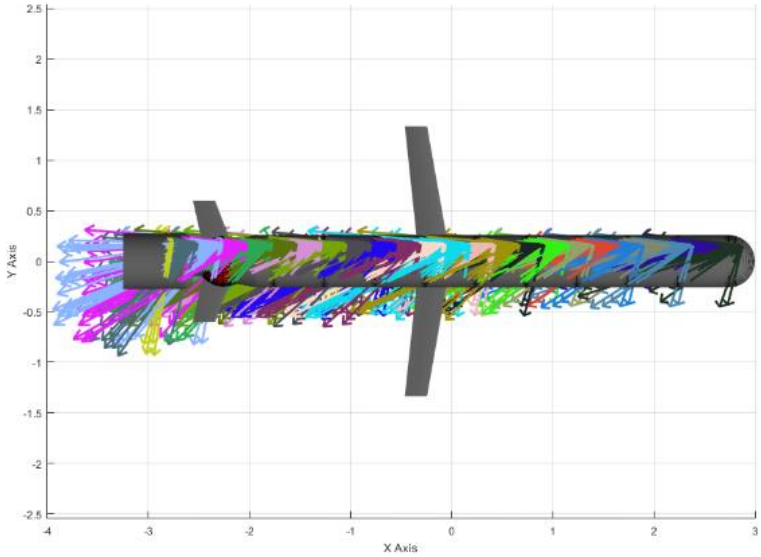

Figure 3.25: Scattering of Striking Fragments at All Detonation Points on XY Axis for the 1^{st} Scenario by Using the Sphere Tool

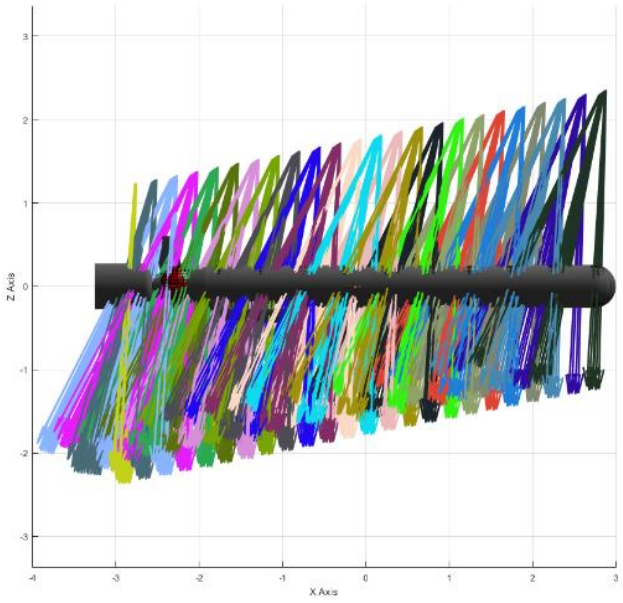

Figure 3.26: Scattering of Striking Fragments at All Detonation Points on XZ Axis for the 1^{st} Scenario by Using the Sphere Tool

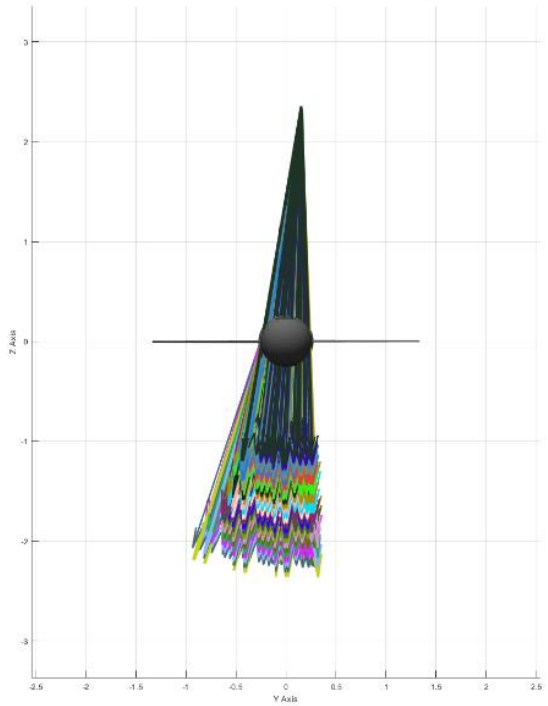

Figure 3.27: Scattering of Striking Fragments at All Detonation Points on YZ Axis for the 1^{st} Scenario by Using the Sphere Tool

Most fragments hit the target at the twenty-second detonation point, as seen in Table 3.13.

The scattering plot of the fragments hitting the target at the twenty-second detonation point can be seen from Figure 3.28, Figure 3.29, and Figure 3.30.

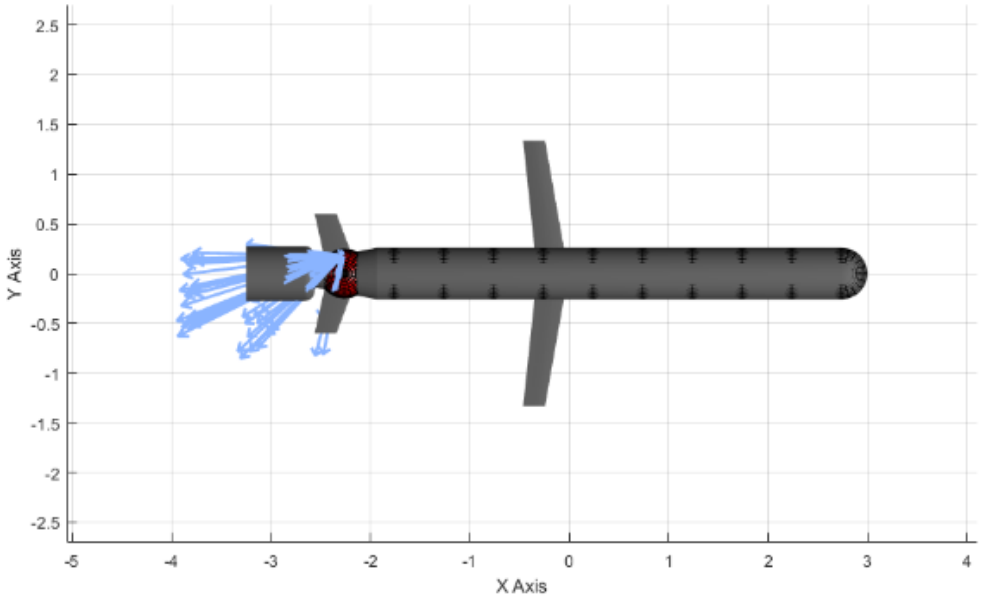

Figure 3.28: Scattering of Striking Fragments at Detonation Point 22 on XY Axis for the 1^{st} Scenario by Using the Sphere Tool

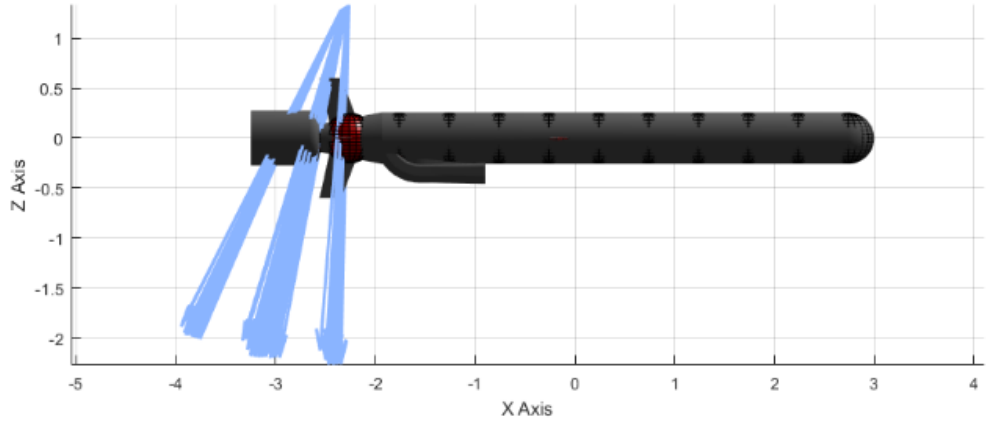

Figure 3.29: Scattering of Striking Fragments at Detonation Point 22 on XZ Axis for the 1^{st} Scenario by Using the Sphere Tool

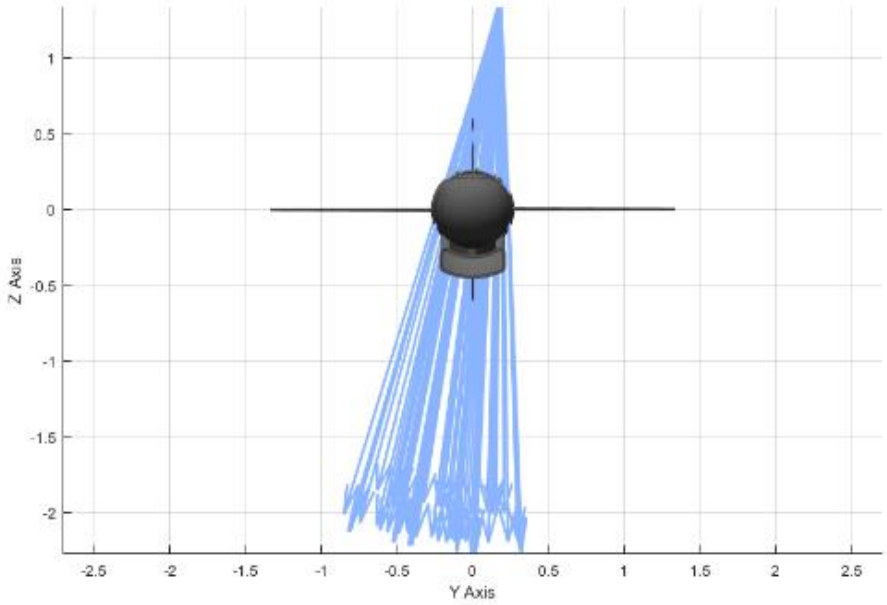

Figure 3.30: Scattering of Striking Fragments at Detonation Point 22 on YZ Axis for the 1^{st} Scenario by Using the Sphere Tool

The number of fragments hitting the target for the first scenario calculated with the tool developed in this thesis and the sphere tool is put in Table 3.14.

Table 3.14: Results Comparison of the Tool Developed in This Thesis and the Sphere Tool

No. of Fragments Hitting the Target wrt Detonation Point	Tool Developed in This Thesis	Sphere Tool
No. of Fragments Hitting the Target @ Detonation Point 1	38	33
No. of Fragments Hitting the Target @ Detonation Point 2	41	26
No. of Fragments Hitting the Target @ Detonation Point 3	41	35
No. of Fragments Hitting the Target @ Detonation Point 4	41	30
No. of Fragments Hitting the Target @ Detonation Point 5	43	33
No. of Fragments Hitting the Target @ Detonation Point 6	46	33
No. of Fragments Hitting the Target @ Detonation Point 7	48	31
No. of Fragments Hitting the Target @ Detonation Point 8	54	37
No. of Fragments Hitting the Target @ Detonation Point 9	81	31
No. of Fragments Hitting the Target @ Detonation Point 10	84	43
No. of Fragments Hitting the Target @ Detonation Point 11	90	32
No. of Fragments Hitting the Target @ Detonation Point 12	101	48
No. of Fragments Hitting the Target @ Detonation Point 13	86	36
No. of Fragments Hitting the Target @ Detonation Point 14	57	50
No. of Fragments Hitting the Target @ Detonation Point 15	55	40
No. of Fragments Hitting the Target @ Detonation Point 16	55	46
No. of Fragments Hitting the Target @ Detonation Point 17	56	45
No. of Fragments Hitting the Target @ Detonation Point 18	57	45
No. of Fragments Hitting the Target @ Detonation Point 19	79	48
No. of Fragments Hitting the Target @ Detonation Point 20	72	45
No. of Fragments Hitting the Target @ Detonation Point 21	95	54
No. of Fragments Hitting the Target @ Detonation Point 22	80	55
No. of Fragments Hitting the Target @ Detonation Point 23	73	39
No. of Fragments Hitting the Target @ Detonation Point 24	57	14
No. of Fragments Hitting the Target @ Detonation Point 25	28	0
No. of Fragments Hitting the Target @ Detonation Point 26	0	0
Total Fragment Number Hitting the Target	1558	929

Since there are spaces between the spheres and the sphere is not placed on the entire surface of the target in the sphere tool, the number of fragments hitting the target is lower than the tool developed in the thesis, as can be seen from Table 3.14. Since the tool developed in the thesis allows processing on the target's entire surface, the results are more realistic, and the warhead detonation point is selected more accurately.

CHAPTER 4

CONCLUSION

In this thesis, a tool is developed for calculating the number of fragments hitting the target when the warhead is exploded. The number of impacting fragments to the target is calculated at regular intervals over a certain distance from the moment the missile detects the target. The target model and the warhead model are created to perform the kill analysis. In addition, 6 DOF simulation output is used for defining missile and target engagement kinematics.

The target model surface is constituted from triangular-shaped patches. Three points of the triangles are known. The plane equation passing through the three points is calculated. Then, fragment velocity and position are evaluated. This enables us to find the fragment vector. The intersection point of the plane and fragment vector is found before deciding the number of fragments hitting to target. If this point is inside the triangle, this fragment is accepted to engage the target.

It is calculated that whether each fragment is inside of each triangle for every detonation point. After finding the detonation point where the maximum number of fragments hit the target, warhead detonation time is decided.

Kill analyses are carried out for different scenarios. The first scenario's target is chosen as a cruise missile, and the second one is selected as a fighter. The tool can be operated for any target type whose solid model is known. Also, kill analysis results are compared for fifteen scenarios with different miss distances. Analysis can be made for millions of different engagement conditions with this tool. Monte Carlo analysis is also performed for the first scenario to examine the effect of uncertainties added to segment limits and fragment speeds on the results. Finally, the tool developed in the thesis is compared with another tool that calculates the number of fragments hitting the target when the warhead is detonated.

As a result of this thesis study, when the most fragments hit the target can be calculated after the missile detects the target thanks to the developed tool, and the warhead will be detonated at that moment, causing more damage to the target and increasing missile lethality.

4.1 Future Work

In future studies,

- Fragment mass and material type can be added to the tool.
- The vulnerability can be considered. If the target model's vital parts are known, the triangles corresponding to these parts can be evaluated as more damaged.
- Since there are many missile-target engagement possibilities in real life, a certain number of analyses can be made, and the results can be based on a function by using an artificial neural network.

REFERENCES

[1] Fair, C. K. (1981). *A Comparison of Computer Warhead-Target Endgame Simulations and Recommendations Pertaining to Future Endgame Programs*. Monterey, California. Naval Postgraduate School.

[2] Arora, V. K. (2010). *Proximity fuzes: Theory and Techniques*. New Delhi: Defence Research and Development Organisation, Ministry of Defence.

[3] Nasser, A., Ahmed, F. M., Moustafa, K. H., & Elshabrawy, A. (2015). *Recent Advancements in Proximity Fuzes Technology*. International Journal of Engineering Research and Technical Research, V4(04). doi:10.17577/ijertv4is041400

[4] Nyongesa, H., Kent, S., & O'keefe, R. (2001). *Genetic Programming for Anti-Air Missile Proximity Fuze Delay-Time Algorithms*. IEEE Aerospace and Electronic Systems Magazine, 16(1), 41-45. doi:10.1109/62.894177

[5] Lei, H., & Hu, Z. (2012). *A Calculation Method of Kill Probability for Air-to-Air Missile.* 2012 Fifth International Symposium on Computational Intelligence and Design. doi:10.1109/iscid.2012.70

[6] Burton, A., Mountford, J., & Garrod, A. (1998). *An Air Target Engagement Simulation for Radar Proximity Fuze Development and Performance Assessment*. IEE Colloquium on Radar System Modelling. doi:10.1049/ic:19980762

[7] Scratchapixel.(2014,August15).RetrievedDecember14,2020,from https://www.scratchapixel.com/lessons/3d-basic-rendering/ray-tracing-rendering-a-triangle/ray-triangle-intersection-geometric-solution

[8] Curless.(2004). *Ray-Triangle Intersection* [Slides]. https://courses.cs.washington.edu/courses/csep557/10au/lectures/triangle_intersection.pdf

[9] Auroux, P. D. Multivariable Calculus (Fall 2010). MIT OpenCourseWare. https://ocw.mit.edu/courses/mathematics/18-02sc-multivariable-calculus-fall-2010/.

[10] Crippin, P., Donato, R., & Kirkpatrick, C. (2009). Calculus and Vectors. Toronto: Nelson Education.